1    **Growth-driven displacement of protein aggregates along the cell length**

2    **ensures partitioning to both daughter cells in *Caulobacter crescentus***

3

4    Frederic D. Schramm[1]\*, Kristen Schroeder[1]\*, Jonatan Alvelid[2], Ilaria Testa[2] and Kristina

5    Jonas[1][§]

6

7    [1] Science for Life Laboratory and Department of Molecular Biosciences, The Wenner-Gren

8    Institute, Stockholm University, 10691 Stockholm, Sweden

9    [2] Science for Life Laboratory and Department of Applied Physics, KTH Royal Institute of

10    Technology, 10044 Stockholm, Sweden

11

12    \* Equal contribution

13    [§] Correspondence: kristina.jonas@su.se, Phone: +46 8 16 2580

## Abstract

All living cells must deal with protein aggregation, which can occur as a result of experiencing stress. In the bacteria *Escherichia coli* and *Mycobacterium smegmatis*, aggregates collect at the cell poles and are retained over consecutive cell divisions only in the daughter cell that inherits the old pole, resulting in aggregation-free progeny within a few generations. Here we have studied the *in vivo* kinetics of aggregate formation and clearance following heat and antibiotic stress in *Caulobacter crescentus*, which divides by a pre-programmed asymmetric cell cycle. Unexpectedly, we find that aggregates do not preferentially collect at the cell poles, but form as multiple distributed foci throughout the cell volume. Time-lapse microscopy revealed that under moderate stress, the majority of protein aggregates are short-lived and rapidly dissolved by the major chaperone DnaK and the disaggregase ClpB. Severe stress or genetic perturbation of the protein quality machinery results in long-lived protein aggregates, which individual cells can only clear by passing on to their progeny. Importantly, these persistent aggregates are neither collected at the old pole over multiple generations nor inherited exclusively by the old pole-inheriting stalked cell, but instead are partitioned between both daughter cells during successive division events in the same ratio. Our data indicate that this symmetric mode of aggregate inheritance is driven by the elongation and division of the growing mother cell. In conclusion, our study revealed a new pattern of aggregate inheritance in bacteria.

2

## Introduction

32

33      Exposure to various types of environmental stress results in the un- and misfolding of proteins,

34      which poses a threat to continued survival. Sudden unfolding of native proteins, as well as

35      interference of un- and misfolded proteins with partially folded species can create a functional

36      deficit which impairs essential cellular processes and may lead to the death of the cell. All forms

37      of life therefore rely on protein quality control systems to prevent accumulation of un- and

38      misfolded proteins. The main participants in these systems are molecular chaperones and

39      proteases that refold or degrade un- and misfolded proteins in order to maintain protein

40      homeostasis as conditions fluctuate (Hartl et al., 2011). Acute stress can lead to exhaustion of

41      the chaperoning and degradation capacity of the cell, resulting in aggregation of proteins that

42      cannot be restored to their native state, either temporarily or indefinitely (Santra et al., 2018;

43      Tyedmers et al., 2010). Sequestering un- or misfolded proteins into more inert particles has

44      been proposed to lead to an immediate easing of the burden on the chaperone machinery, and

45      can even be chaperone driven (Grousl et al., 2018; Ungelenk et al., 2016).

46      How cells cope with protein aggregates can differ depending on the type and amount of

47      aggregated proteins present, but the highly conserved chaperone systems are responsible for

48      effecting survival. Small heat shock proteins (sHSPs) associate with aggregated protein to

49      maintain it in a refolding-competent state and can also promote the fusion of aggregates and

50      facilitate their resolution (Coelho et al., 2014; Specht et al., 2011; Ungelenk et al., 2016). The

51      cytoplasmic DnaK/Hsp70 chaperone and the ClpB/Hsp104 disaggregase bind insoluble

52      aggregates and work in concert on their dissolution, returning proteins to their folded state

53      (Glover and Lindquist, 1998; Goloubinoff et al., 1999). Additionally, cytosolic proteases

54      contribute to aggregate resolution through the degradation of the constituent proteins (Heck et

55      al., 2010; Tomoyasu et al., 2001).

56  If aggregates persist for a prolonged time and remain even after conditions improve,

57 asymmetric distribution of insoluble deposits to daughter cells has been suggested to provide

58 an effective means of sequestering un- and misfolded protein from a part of the population (Hill

59 et al., 2016; Lindner et al., 2008; Vaubourgeix et al., 2015; Vedel et al., 2016; Winkler et al.,

60 2010). For example, the budding yeast *Saccharomyces cerevisiae* retains aggregates in the

61 mother cell both by active and passive mechanisms to generate aggregate-free daughter cells

62 (Erjavec et al., 2007; Higuchi et al., 2013; Spokoini et al., 2012; Zhou et al., 2011). Although

63 accumulation of protein aggregates has generally been associated with cell ageing and other

64 pathology (Aguilaniu et al., 2003; Mogk et al., 2018; Nyström and Liu, 2014; Shcheprova et

65 al., 2008), several recent studies suggest that the carriage of persistent protein aggregates may

66 also confer a fitness advantage and promote survival (Govers et al., 2018; Saarikangas and

67 Barral, 2015; Wallace et al., 2015).

68  So far, most studies addressing the *in vivo* dynamics of protein aggregate formation and

69 clearance have been performed in eukaryotes. However, bacteria in particular frequently

70 encounter stress conditions that perturb protein homeostasis, including heat, oxidative or

71 antibiotic stress. In *Escherichia coli*, protein aggregates mostly accumulate at the chromosome-

72 free polar regions of the cell (Kumar and Sourjik, 2012; Winkler et al., 2010). With successive

73 cell divisions, this localization rapidly results in the production of aggregate-free cells (Govers

74 et al., 2014; Lindner et al., 2008; Winkler et al., 2010). Similarly, slow-growing *Mycobacteria*

75 were shown to collect irreversibly damaged proteins at the pole and distribute them

76 asymmetrically to progeny, again resulting in aggregate-free daughter cells upon cell division

77 (Fay and Glickman, 2014; Vaubourgeix et al., 2015). In both *E. coli* and *Mycobacterium*, the

78 carriage of ancestral protein aggregates has been associated with a decline in growth rate

79 (Lindner et al., 2008; Vaubourgeix et al., 2015; Winkler et al., 2010). However, a more recent

80 study argues that *E. coli* cells inheriting protein aggregates along with components of the

81      protein quality control machinery show an increased robustness to subsequent proteotoxic

82      stress (Govers et al., 2018). Despite insight into the strategies and physiological consequences

83      of aggregate distribution employed by *E. coli* and *Mycobacteria*, it remains poorly understood

84      how other bacteria deal with protein aggregates in response to changing growth conditions. Of

85      particular interest is how protein aggregation is handled by bacterial species possessing an

86      intrinsically asymmetric life cycle, generating daughter cells with distinct cell fates.

87          The α-proteobacterium *Caulobacter crescentus* has long been a model organism of

88      bacterial cell type differentiation as it undergoes asymmetric cell division. Each division cycle

89      of *C. crescentus* yields two non-identical daughter cells, a motile, non-replicative swarmer cell,

90      and a surface-attached and replication competent stalked cell (Curtis and Brun, 2010). As a

91      free-living aquatic bacterium, it frequently encounters temperature fluctuations and other

92      stresses that potentially threaten the folding state of the protein complement. A previous report

93      has suggested that *C. crescentus* stalked cells undergo a slow replicative aging (Ackermann et

94      al., 2003). While in yeast, replicative ageing has been attributed to an accumulation of protein

95      aggregation in the mother cell (Aguilaniu et al., 2003; Coelho et al., 2014; Erjavec et al., 2007;

96      Hill et al., 2014), the observed decline in the reproductive output of *C. crescentus* remains

97      largely unexplained. Major components of the general chaperone machinery of *C. crescentus*

98      have been described and their importance for stress resistance is known (Baldini et al., 1998;

99      Da Silva et al., 2003; Schramm et al., 2017). However, to date it has not been studied how *C.*

100     *crescentus* manages protein aggregation during its asymmetric life cycle, and the question

101     persists if retention of protein damage in the stalked cell may explain the previously observed

102     ageing effects.

103         In this study we have followed the dynamics of aggregate formation, clearance and

104     inheritance following heat and antibiotic stress and recovery in *C. crescentus*. We demonstrate

105     that protein aggregates form as multiple DnaK-attended foci throughout the cell volume and

5

106    that the mechanism by which cells clear aggregates largely depends on the intensity of stress.

107    Importantly, we show that in contrast to previously studied bacteria, persistent aggregates that

108    form as a consequence of severe stress or genetic mutation do not sort to the old pole-containing

109    stalked cell, but are instead distributed to both daughter cells at the same ratio over successive

110    divisions.

## Results

**Heat and antibiotic stress induce relocalization of the *C. crescentus* chaperone machinery to foci of protein aggregation.**

In order to probe the dynamics and requirements of protein aggregation and resolution in *C. crescentus*, we constructed strains bearing fluorescently-tagged versions of the major heat shock chaperone DnaK and the bacterial disaggregase ClpB, at their respective native loci (Fig. 1A). Tagging these proteins did not result in viability defects at the optimal growth temperature of 30°C, although expressing the tagged version of ClpB correlated with a reduction in heat tolerance (Supporting Information Fig. 1). We found that DnaK tagged with the monomeric fluorescent protein mVenus (DnaK-mVenus) was diffusely localized throughout cells at a normal growth temperature of 30°C (Fig. 1B). To probe the localization of DnaK-mVenus at super-resolution, we imaged cells with stimulated emission depletion (STED) microscopy and found that the diffuse pattern of DnaK-mVenus at 30°C was representative of many small clusters of DnaK measuring $66 \pm 23$ nm (Fig. 1C). Upon exposure to a heat stress temperature of 40°C, DnaK-mVenus localization changed to a punctate pattern, suggesting that in *C. crescentus* protein aggregation is grouped into multiple foci that are distributed throughout the cell volume (Fig. 1B). Most cells contained between two and four DnaK-mVenus foci, while around 10% of the population harbored five or more foci (Fig. 1D). STED imaging of the foci formed during heat shock revealed large foci that measured $199 \pm 56$ nm (Fig. 1C). Determining the cellular position of DnaK-mVenus clusters showed that they occur with similar frequency along the cell length (Fig. 1E).

Disabling ATP hydrolysis of DnaK by introducing a K70A mutation (Barthel et al., 2001) largely prevented DnaK from relocalizing to foci during heat stress, confirming that stress-induced DnaK relocalization is a function of its ATP-dependent foldase activity (Fig. 1F). To test whether the observed DnaK foci correspond to sites of protein aggregation, we

7

136    used the aggregation-prone ELK16 peptide fused to mCherry as a marker for protein

137    aggregation (Wu et al., 2011), and saw colocalization between DnaK-mVenus and mCherry-

138    ELK16 foci after heat stress (Fig. 1B). Finally, co-localization experiments with the ClpB-

139    mCerulean reporter showed that following exposure to heat stress ClpB attends mostly the same

140    foci as DnaK-mVenus and mCherry-ELK16 (Fig. 1B), while no fluorescence was observed for

141    the ClpB reporter at the normal growth temperature, in keeping with its heat shock-dependent

142    expression (Simão et al., 2005). We note that ClpB foci were fewer and that some of the less

143    intense foci of DnaK and mCherry-ELK16 were not attended by ClpB (Fig. 1B). This

144    observation may be attributable to the function of ClpB in assisting refolding of large

145    aggregates (Mogk et al., 2003b) or the reduced functionality of the ClpB-mCerulean fusion

146    (Supporting Information Fig. 1). In addition to DnaK, ELK16 and ClpB, we have also tagged

147    the small heat shock protein homolog CCNA_02341 (hereafter referred to as sHSP1). However,

148    tagging this protein resulted in increased heat sensitivity, the formation of atypically large

149    fluorescent clusters, and cell division defects during mild heat stress (Supporting Information

150    Fig. 1). Based on these experiments we decided to utilize DnaK-mVenus for the visualization

151    of aggregate localization throughout this study.

152        To determine the relationship between aggregate foci and the *Caulobacter*

153    chromosome, we stained the DNA using Hoechst 33258 in the DnaK-mVenus reporter strain

154    sampled at normal temperature as well as after heat shock (Fig. 1G). Surprisingly, aggregate

155    formation during heat shock was accompanied by a change in the spatial organization of the

156    DNA from an evenly dispersed to a patchy pattern. Moreover, the locations occupied by protein

157    aggregates corresponded to regions of reduced DNA staining intensity. These data suggest that

158    in contrast to *E. coli* and other bacteria, in which the chromosome pushes aggregates to the cell

159    poles (Coquel et al., 2013; Lindner et al., 2008; Winkler et al., 2010), in *Caulobacter* protein

160    aggregates appear to displace the chromosome.

161    Aggregate formation was observed at heat shock temperatures of 40°C and 45°C (Fig.

162    1H), but also upon exposure to sublethal concentrations of kanamycin, which is known to

163    induce protein aggregation through mistranslation in *E. coli* (Kohanski et al., 2008). STED

164    imaging revealed that kanamycin-induced aggregates were smaller than those induced by heat

165    shock, forming as foci measuring $127 \pm 39$ nm (Fig. 1C). No aggregation foci were observed

166    following treatment with the antibiotic fosfomycin, which blocks production of peptidoglycan

167    precursors, nor for spectinomycin (Fig. 1H), a ribosome-binding aminoglycoside that does not

168    cause mistranslation (Kohanski et al., 2008).

169    Finally, our reporter strains also allowed us to quantify the induction of *dnaK* expression

170    following stress exposure by determining the fluorescence intensity per bacterial pixel in

171    different conditions (Fig. 1I). Exposure to 40°C for one hour induced a four-fold increase in

172    DnaK levels, while a temperature of 45°C induced a two-fold increase within one hour, which

173    we confirmed by western blotting (Fig. 1J). Although strong aggregation was present, lower

174    induction of DnaK at 45°C and following kanamycin treatment is possibly due to lower

175    translation capacity in these conditions (Chen et al., 2017). Treatment with fosfomycin or

176    spectinomycin did not increase DnaK levels, indicating that the inhibitory effects of these

177    antibiotics act independently of protein aggregation and the heat shock response in *C.*

178    *crescentus* (Fig. 1I, J). Altogether, these data establish that protein aggregation occurs at

179    multiple sites in *C. crescentus* and that the major chaperones DnaK and ClpB are recruited to

180    these sites.

181

182    **Proteins governing diverse processes comprise aggregate foci in *C. crescentus*.**

183    Having established a system for visualizing total cellular aggregation, we next asked

184    what proteins might be un- or misfolding, thereby recruiting DnaK to foci of aggregation. In

185    order to address this question, we isolated insoluble detergent-resistant proteins from wild type

9

186    *C. crescentus* grown at 30°C or exposed to a stress temperature of 45°C for 1 hour, subjected

187    them to mass spectrometry, and identified 133 proteins enriched specifically in the aggregated

188    fraction during heat stress (Fig. 2A, Supporting Information Tab. 2). Comparing the abundance

189    of aggregate-enriched proteins sorted by functional category (Fig. 2B), showed that proteins

190    belonging to various cellular processes become associated with the aggregate foci, including

191    54 essential proteins (Supporting Information Tab. 2). The most abundant protein in the

192    aggregated fraction was sHSP1, which shares 54% and 40% amino acid sequence homology

193    with the *E. coli* small heat shock proteins IbpA and IbpB, respectively. This result is consistent

194    with a previously described role of small heat shock proteins in binding and maintaining un- or

195    misfolded proteins in a disaggregation-ready state (Lindner et al., 2008; Mogk et al., 2003a;

196    Strozecka et al., 2012).

197        To verify the identity of aggregated proteins detected by mass spectrometry, we selected

198    the proteins GyrB, FusA, and the predicted homocysteinase CCNA_00257 to monitor their

199    subcellular localization when exposed to heat and kanamycin stress (Fig. 2C). All three proteins

200    were confirmed to condense into aggregate foci colocalizing with DnaK when exposed to stress

201    (Fig. 2C). Interestingly, in contrast to GyrB, which relocalized in the majority of cells during

202    all exposures, the number of cells with CCNA_00257 and FusA aggregates differed depending

203    on the stress signal (Fig. 2D). While heat stress induced foci formation by CCNA_00257 in

204    nearly all cells, kanamycin treatment resulted in foci formation in only 15% of the population,

205    indicating that CCNA_00257 is less sensitive to kanamycin-induced effects than GyrB. FusA

206    only relocalized into aggregate foci in 20% of the population during heat stress, again indicating

207    that individual proteins are destabilized by different stress exposures. Collectively our data

208    show that proteins belonging to diverse cellular processes become members of the aggregate

209    foci observed in *C. crescentus* and that the composition of aggregates is dependent on the stress

210    condition.

211

**Contribution of major chaperones and proteases to stress resistance and aggregate dissolution.**

214      In order to maintain cellular protein homeostasis, chaperones and proteases forming the protein quality control machinery must cooperate in protein folding, aggregate resolution, and degradation of un- and misfolded proteins. Through a series of deletion mutants we probed the contribution of ClpB, sHSP1, the other small heat shock protein homolog CCNA_03706 (hereafter referred to as sHSP2), and the protease Lon to aggregate resolution and stress resistance in *C. crescentus*.

220      In accordance with low expression during normal growth temperature, deletion of *clpB*, *shsp1*, and *shsp2* had no discernible effect at 30°C (Fig. 3A, B). Upon heat stress, the viability of cells lacking ClpB was drastically reduced, as has been demonstrated previously (Simão et al., 2005). The number and distribution of DnaK foci was similar to that observed in the presence of ClpB, however even when challenged by a sublethal heat shock cells were still unable to resolve aggregated protein deposits, which instead persisted over many generations even after release from stress (Supporting Information Fig. 2). In contrast to this pronounced phenotype, absence of *shsp1* or *shsp2* alone or in combination had no effect on resistance to heat treatment (Fig. 3A). The overall pattern of protein aggregation was unchanged in the absence of the sHSPs, forming still as distributed punctate foci, and aggregates were resolved within the same time frame as the parental strain (Fig. 3B). Basal levels of DnaK as well as levels induced by heat stress were similar in the absence of the sHSPs (Fig. 3C), indicating that additional DnaK is not compensating for the activity of these proteins and that although sHSP1 comprises nearly half of the aggregated protein fraction, both sHSPs are largely dispensable for tolerating acute heat stress under the stress conditions tested.

235       Proteases support foldases in maintaining protein homeostasis by degrading un- or

236    misfolded proteins, and combined loss of proteases has been shown to induce strong defects in

237    protein quality control (Kanemori et al., 1997). Lon is generally viewed as the major protein

238    quality control protease in *E. coli* (Rosen et al., 2002; Van Melderen and Aertsen, 2009), and

239    has a role in cell cycle control and responding to unfolded protein in *C. crescentus* (Jonas et al.,

240    2013). Cells lacking Lon exhibited only slight reduction in viability during heat stress (Fig.

241    3A), and both *dnaK-mVenus* induction and the pattern of aggregation occurred as when Lon

242    was present. Additionally, in the absence of Lon cells were able to completely dissolve protein

243    aggregates within a similar time frame as the parental strain (Fig. 3B, C). Thus, the Lon protease

244    is not required for resolving protein aggregation under these stress conditions.

245        Together our data demonstrate that clustering of protein aggregation into several smaller

246    foci and the recruitment of DnaK to these sites does not depend on other heat shock proteins.

247    Furthermore, our data confirm in *C. crescentus* that resolution of protein aggregates requires

248    the disaggregase ClpB and the chaperone DnaK, and that despite the heat shock induction of

249    sHSPs and Lon, these factors are dispensable under the conditions tested.

250

251    **Aggregate clearance through dissolution or dilution is dictated by stress severity**

252        As we have identified aggregate composition as well as chaperone contributions to

253    aggregate dissolution, we next wanted to determine how *C. crescentus* responds to protein

254    aggregation provoked by different stress intensities and how aggregates are cleared following

255    shift to non-stress conditions. We therefore used fluorescence time-lapse microscopy to follow

256    aggregate formation and resolution dynamics during different stress exposures.

257        To analyze the formation of aggregates following a temperature upshift, we transferred

258    cultures grown at the normal temperature of 30°C to agarose pads and placed them into the

259    imaging system pre-heated to either 30, 40, or 44°C, and monitored the localization pattern of

12

260    DnaK-mVenus as a proxy for aggregate formation over time (Fig. 4A). Under both heat shock

261    conditions, we observed rapid formation of an average of 3.7 aggregates per cell within 10 min

262    of heat exposure (Fig. 4A, B, Supporting Information Movie 1). During incubation at 40°C,

263    cells grew into microcolonies which increased in area at a rate similar to those in non-stress

264    conditions, and aggregate formation and dissolution appeared highly dynamic (Fig. 4B, C).

265    After their initial appearance the foci number per cell was quickly reduced until reaching a

266    plateau of approximately one aggregate per cell by approximately two hours. We observed that

267    the lifespan of most aggregates was less than 10 min (Fig. 4D). Only 23% of aggregates

268    persisted for more than two hours (Fig. 4D), demonstrating that the aggregate numbers

269    following two hours of exposure to 40°C represent a steady state of formation and

270    disappearance of mostly short-lived aggregates as cells grow, with a minority of persistent

271    aggregates emerging. We attribute the initial net reduction of aggregate number per cell (Fig.

272    4B) to continued growth and division and rapid induction of heat shock gene expression, which

273    allows cells a greater capacity to cope with higher amounts of unfolded protein present at the

274    new elevated temperature (Fig. 4E).

275        Although microcolonies grew at a relatively normal rate, we observed that temperatures

276    near 40°C resulted in abnormal filamentous growth phenotypes, indicative of cell division

277    defects (Fig. 4F), consistent with an earlier study (Heinrich et al., 2016). At a temperature of

278    44°C cell growth was essentially arrested (Fig. 4A, C) while DnaK-mVenus levels drastically

279    increased over time, indicating strong and persistent induction of heat shock gene expression

280    (Fig. 4E). We observed that DnaK foci slowly dissolved until only 40% remained after 6 to 8

281    hours of exposure to 44°C, and only rarely observed the formation of new aggregates at this

282    temperature (Fig. 4B, G). This observation indicates that a fraction of aggregates can be

283    resolved by the highly abundant chaperones, or that DnaK is released from persistent aggregates

284    under this severe continuous stress.

285    To monitor the resolution of aggregates as cells recovered from heat stress, we exposed

286    cells growing in liquid culture to 40, 42, 44 or 46°C for one hour, followed by transfer to agarose

287    pads for imaging at 30°C (Fig. 5A, Supporting Information Fig. 3). During recovery from these

288    temperatures some or all of the stress-treated population remained capable of resuming growth

289    (Fig. 5B) and reducing the average number of aggregates per cell (Fig. 5C). How quickly the

290    average number of aggregates was reduced and whether this was accomplished by aggregate

291    dissolution or dilution within a growing microcolony was dependent on the severity of the heat

292    stress. Growth resumption and aggregate reduction were equally fast in cells exposed to 40 and

293    42°C (Fig. 5B, C), where all protein aggregates were completely dissolved within one hour

294    (Fig. 5C), leading to aggregate-free microcolonies (Fig. 5A, D). In contrast, cells recuperating

295    from exposure to 46°C showed a strong growth delay and decreased ability to clear aggregates,

296    and were heterogenous both in aggregate resolution and the ability to produce normally growing

297    progeny (Fig. 5A, B, D, E). Only 25% of cells were able to produce microcolonies of normally

298    sized progeny (Fig. 5D), in which the average aggregate number per cell was notably reduced

299    (Fig. 5C, E). The remaining 75% of the population were either unable to resume growth within

300    4.5 hours (32%) or resumed growth with varying degrees of division defects (43%) (Fig. 5D).

301    Importantly, although most individuals within the forming microcolonies became eventually

302    aggregation-free, a fraction of offspring maintained aggregates. Many of these aggregates

303    originated from the heat exposed mother cell and persisted for the duration of imaging.

304    However, we also observed that a fraction of new shorter-lived aggregates formed during

305    recovery (Fig. 5F). Based on these analyses we conclude that a portion of aggregates formed

306    during 46°C exposure persist over several generations and are cleared from individual cells

307    mainly through dilution within the microcolony rather than dissolution. A similar behavior was

308    also observed after exposure to 40°C for 10 min in the Δ*clpB* strain, where despite efficient

14

309    clearance of aggregates from individual cells, all aggregates were long-lived (Supporting

310    Information Fig. 2).

311         When monitoring the recovery of cells following exposure to 44°C we again observed

312    that aggregates are cleared through a combination of dissolution and dilution (Supporting

313    Information Fig. 4). However, in contrast to the 46°C condition, the fraction of cells able to

314    produce normally sized progeny was larger (77%) (Fig. 5F), cells resumed growth earlier (Fig.

315    5B) and nearly all cells were free of protein aggregates by 4.5 hours after exposure (Fig. 5C).

316         Taken together our results demonstrate that the severity of heat stress determines the

317    way by which aggregates are cleared from the cell. Following exposure to moderate stress,

318    virtually all aggregates are rapidly dissolved by the protein quality control machinery. By

319    contrast, aggregate clearance following severe stress depends more on dilution during cell

320    division. Consequently, an inability to resume growth and cell division following such severe

321    stress prevents successful aggregate clearance.

322

323    **The aggregate load does not sort to swarmer or stalked daughter cells in *C. crescentus*.**

324         Asymmetric inheritance of protein aggregates has been proposed to underpin the

325    senescence of aggregate retaining cells and the rejuvenation of aggregate free cells (Ackermann

326    et al., 2003; Coelho et al., 2014; Lindner et al., 2008; Shapiro et al., 2002; Winkler et al., 2010).

327    While asymmetric inheritance in *E. coli* and *Mycobacteria* takes place through collection of

328    aggregates at the poles, in budding yeast asymmetric inheritance is achieved through retention

329    in the much larger mother cell. Since *C. crescentus* has a pre-programmed asymmetric division

330    cycle yielding a bigger stalked/old pole and a smaller swarmer/new pole cell, we sought to

331    understand how persistent aggregates are inherited in this organism.

332         To study aggregate inheritance when only dilution can be used as a means of aggregate

333    clearance, we made use of the Δ*clpB* background to investigate the distribution of aggregates

15

334    following division. A short heat shock of 10 minutes at 40°C induced formation of persistent

335    protein aggregates in this strain that were distributed throughout the cell volume, while the

336    ability to grow and divide was preserved (Supporting Information Fig. 2), therefore we followed

337    the inheritance of these aggregates over consecutive cell divisions by time lapse microscopy

338    (Fig. 6A). A kymograph normalized to the summed length of all descendants from one

339    individual cell shows that aggregates are relatively static and rarely change their cellular

340    position between two cell division events (Fig. 6B). However, establishment of new cell

341    boundaries as a consequence of cell division affected the relative cellular position of aggregates;

342    for example, an aggregate located at midcell of a stalked cell becomes located closer to the new

343    pole in the daughter cell following division (Fig. 6A, B). To analyze the positional change of

344    aggregates more quantitatively, we determined the frequency by which aggregates obtain a new

345    cellular position in the daughter stalked cell after cell division, as a function of their original

346    cellular position (Fig. 6C, Supporting Information Fig. 5). Consistent with the kymograph

347    analysis, these data show that aggregates located at midcell in the mother cell were likely to

348    change relative position (71%) during cell division to become closer to the new pole of the

349    stalked daughter cell. Aggregates between the old pole and midcell (classified as old pole half)

350    either maintained their original relative position (64%) or also obtained a new relative position

351    close to the new pole (34%). By contrast, aggregates located at the pole of the mother cell

352    generally maintained their position during cell division (90%) and changed to a position closer

353    to the new pole in only 10% of cases. Importantly, we only very rarely observed that aggregates

354    located outside pole regions became situated closer to the old pole as a consequence of cell

355    division (2% and 3% of those in the old pole half or at midcell, respectively), indicating that

356    essentially all aggregates that obtain a new relative position in the daughter stalked cell after

357    division, are situated closer to the new pole. We explain this passive "movement" of aggregates

358    towards the new pole with the growth mode of *C. crescentus*, in which cells grow along the cell

16

359    length, excluding the poles (Aaron et al., 2007; Lambert et al., 2018). Consequently, the fraction

360    of aggregates originally formed at the poles will remain there over generations due to the

361    absence of cell elongation in this area. Therefore, the majority of aggregates, while static, are

362    displaced in proportion to the elongation of the cell and maintain their relative position until a

363    division event sets new cellular boundaries (Fig. 6D).

364        The result that cell growth and the establishment of new cell boundaries during division

365    frequently resulted in aggregates becoming closer to the new pole suggested that with

366    consecutive divisions, these aggregates would eventually be inherited by a swarmer cell.

367    Consistent with this hypothesis, we found that the cellular position in the mother cell largely

368    determines to which daughter cell aggregates are distributed (Fig. 6E). Nearly all aggregates at

369    the new pole or in the new pole half were inherited by the daughter swarmer cell, while

370    essentially all aggregates at the stalked pole or in the old pole half were inherited by the

371    daughter stalked cell (Fig. 6E). Aggregates with an original location around midcell were either

372    inherited by the daughter stalked (74%) or swarmer (26%) cells. The preference towards the

373    stalked cell may be attributable to the size difference between stalked and swarmer cells (Fig.

374    6F).

375        In sum, our data show that the cellular positioning of aggregates in *C. crescentus* is

376    largely governed by the elongation of the cell and the placement of the division plane, and that

377    the cellular position of aggregates in a mother cell determines the likelihood of being inherited

378    by a particular cell type. As such, it is unlikely that *C. crescentus* accumulates aggregates in the

379    old pole-inheriting daughter cell, as previously shown for *E. coli* and *Mycobacterium* (Lindner

380    et al., 2008; Vaubourgeix et al., 2015; Winkler et al., 2010). To test this idea more directly, we

381    determined the percentage of total aggregates that are distributed to either the old pole-

382    inheriting stalked or the new pole-inheriting swarmer cell through five division events.

383    Consistently, we found that the fraction of aggregates inherited by either cell type was stable

17

384    (Fig. 6G). Likewise, the fraction of polar aggregates remained stable at approximately 30%

385    over multiple generations (Fig. 6H). Stalked cells always inherited more aggregates than

386    swarmer cells (70%) (Fig. 6G), which we attribute to the size difference and the observation

387    that it is the stalked cell that inherits the old pole (Fig. 6C, F).

388        Collectively, our data show that persistent protein aggregates in *C. crescentus* are

389    neither collected at the old pole nor asymmetrically distributed to only the stalked cell; rather,

390    both daughter cells inherit aggregates at a constant ratio. In addition to our analysis of the Δ*clpB*

391    background, we also investigated how persistent aggregates (Fig. 4D) are inherited in wild type

392    cells during sustained stress at 40°C and during recovery from 44°C (Supporting Information

393    Fig. 6, 7). These experiments yielded similar results to that obtained in the Δ*clpB* strain (Fig.

394    6), confirming that under these conditions *C. crescentus* does not rely on asymmetric

395    inheritance of protein aggregates towards one cell type.

## Discussion

Our study describes the dynamics of protein aggregate formation and clearance in response to antibiotic and heat stress in the asymmetrically dividing bacterium *C. crescentus*. We find that while utilizing the same key players for aggregate clearance as other bacteria, how aggregates form in *C. crescentus* and how they are partitioned during division differs from previously described bacteria.

**Subcellular localization of aggregate clusters**

We demonstrate that multiple foci of protein aggregation form in *C. crescentus* throughout the cell volume in response to both antibiotic and heat stress. In *Mycobacterium* protein aggregates also form as multiple distributed foci, although these are collected at the cell pole within one doubling time to form a pattern similar to that of *E. coli*, where aggregates rapidly localize at the poles after formation (Coquel et al., 2013; Lindner et al., 2008). In *E. coli,* it has been demonstrated that the condensed nucleoid governs collection of bigger aggregates through macromolecular crowding, enforcing movement towards and deposition at the poles (Coquel et al., 2013; Winkler et al., 2010). Compared to *E. coli* (Winkler et al., 2010), *C. crescentus* shows a more relaxed arrangement of the chromosome, where the nucleoid fills the entire cell volume (Fig. 1G). We suspect that this pattern might allow aggregate deposition throughout the entirety of the cell as opposed to only at the poles. Other large subcellular structures, such as polyphosphate granules, have been demonstrated to occupy particular locations within the cell (Henry and Crosson, 2013), however our analysis did not reveal that aggregates were more or less associated with particular cellular positions.

As cells begin to grow, whether in the presence of constant sublethal stress or during recovery from acute heat shock, we found that the majority of persistent aggregates, while static, are displaced in proportion to the elongation of the cell. We demonstrate that this

19

421    displacement is continuous, although cell division may dictate a new relative position within

422    the daughter cell. As heat shock-induced aggregates are very large and can nearly span the

423    entire width of the cell, we expect that these may be resistant to movement within the cell, and

424    would be largely unaffected by the movement of smaller, more mobile cellular components.

425    Alternatively, the incorporation of un- or misfolded membrane anchored proteins into aggregate

426    clusters may restrict intracellular movement, as has been demonstrated in *E. coli* when

427    aggregation-prone luciferase attached to a membrane anchor is expressed (Winkler et al., 2010).

428    In support of this latter hypothesis, we detected several membrane-associated cellular proteins

429    to be enriched in the aggregate fraction during severe heat stress, suggesting a potential means

430    of "tethering" the aggregate and restricting its diffusion throughout the cell.

431

432    **Aggregate clearance in response to different stress intensities**

433            While the pattern of aggregate formation in *C. crescentus* was similar throughout all

434    tested stress conditions, we found that the mechanisms by which aggregates are removed from

435    individual cells largely depend on the type and intensity of stress. When recovering from

436    exposure to sublethal stress, aggregates are rapidly dissolved by the combined activity of DnaK

437    and ClpB resulting in complete aggregate clearance from the population within one generation.

438    Furthermore, we found that *C. crescentus* is able to cope with continuous exposure to 40°C by

439    rapidly upregulating the heat shock response following temperature upshift, leading to a new

440    homeostasis of aggregate formation and dissolution, with more persistent aggregates being

441    diluted through continuous cell growth. Noticeably, although cells incubated at 40°C grow at a

442    similar rate as unstressed cells, they become elongated, indicating defects or delays in

443    completing the cell cycle. A previous study showed that the cell cycle regulator CtrA is

444    downregulated under this condition (Heinrich et al., 2016).

20

445   Our data show that when *C. crescentus* is subjected to intense stress, the persistent

446   aggregates that form cannot be dissolved by the major chaperones, indicating that under these

447   conditions the capacity of the protein quality control machinery is exhausted. The only way to

448   reduce these persistent aggregates in individual cells is to distribute them during the process of

449   cell division. Consequently, only growing and dividing cells can remove persistent aggregates,

450   while those cells that arrest growth maintain them. Our data demonstrate that exposure to severe

451   stress is associated with a marked heterogeneity in the ability to return to normal growth, with

452   only a fraction of the population returning to normal growth following release to non-stress

453   conditions. We expect that massive aggregation under severe stress causes disruption of

454   numerous essential growth processes, supported by previous studies which indicate that strong

455   heat shock response induction during the severe unfolding stress of high temperatures directs

456   cellular resources away from protein translation to survival functions (Chen et al., 2017; Santra

457   et al., 2017; Schramm et al., 2017).

458

459   **Pattern of aggregate inheritance and its physiological consequences**

460   Our finding that persistent aggregates do not accumulate in the stalked cell, but are

461   instead distributed to both daughter cells at a stable ratio, unveils that the pattern of aggregate

462   inheritance strikingly differs between *C. crescentus* and the previously studied bacteria *E. coli*

463   and *Mycobacterium*. In the latter cases, aggregates are retained only in the old pole-inheriting

464   daughter cell, whereas the daughter cell inheriting the new pole escapes inheritance of

465   aggregate foci (Govers et al., 2018; Lindner et al., 2008; Vaubourgeix et al., 2015; Vedel et al.,

466   2016; Winkler et al., 2010). The resulting heterogeneity of growing microcolonies, in which

467   one part of the population carries protein aggregates while the other part does not, has been

468   suggested to provide a benefit for the population, either by providing a source of rejuvenation

469   (Lindner et al., 2008; Winkler et al., 2010) or by increasing robustness to subsequent stresses

470   (Govers et al., 2018).

471        An asymmetric pattern of aggregate inheritance has been a plausible, though untested,

472   explanation for the previous observation that *Caulobacter* stalked cells decrease reproductive

473   output with increasing cell age (Ackermann et al., 2003). While a minority of aggregates were

474   trapped at the poles in *Caulobacter*, additional aggregates did not accumulate at this location,

475   with the majority of cells instead eventually passing their aggregate content on to swarmer cells.

476   Our findings suggest that rather other reasons, for example retention of older membrane

477   components (Bergmiller et al., 2017), may underlie the phenomenon of stalked cell senescence.

478        Taken together, our work has revealed for the first time a shared mode of aggregate

479   inheritance in bacteria, highlighting that asymmetric aggregate inheritance is not the sole way

480   of managing protein aggregation. If *C. crescentus* benefits from the observed slow distribution

481   of persistent aggregates to both daughter cell types is unclear. However, it may be advantageous

482   to preserve both cell types in the population rather than sacrifice one type for the other in the

483   ever-changing aquatic habitat of this bacterium.

## Materials and Methods

### Growth conditions

*C. crescentus* strains were routinely grown at 30°C in liquid PYE medium in either an Infors HT Multitron Standard or Infors HT Ecotron rotating shaker set to 200 rpm, or on solid PYE agar. Prior to analysis, all liquid cultures were grown undisturbed in exponential phase at 30 °C for three hours to allow any aggregation from other sources to be resolved or diluted. Heat shock experiments were performed by moving 100 ml flasks of 10 ml cultures growing at 30°C to a shaking incubator pre-heated to the desired temperature. Media were supplemented with the following additives when indicated; xylose 0.3 %, vanillate 500 µM. Antibiotics were used at following concentration (concentration in liquid/solid media as µg/mL): kanamycin 5 (2.5 in the case of KJ956 and KJ957)/25, spectinomycin 25/400, gentamycin 0.625/5, tetracycline 1/2, rifampicin 2.5/5. Experiments were generally performed in the absence of antibiotic when using strains in which the resistance cassette was integrated into the chromosome. *E. coli* strains for cloning purposes were grown in LB medium at 37°C, supplemented with antibiotics at following concentrations: kanamycin 30/50, spectinomycin 50/50, gentamycin 15/20, tetracycline 12/12, rifampicin 25/50. Details on strain and plasmid construction are reported in Supporting Information Text 1 and Supporting Information Tab. 1.

### Microscopy

To visualize cells, a 1% agarose in PYE slab was poured using a GeneFrame (Thermo Fisher Scientific) attached to a glass slide and coverslip, which was pre-warmed to 30°C prior to all experiments. At the indicated time points, a small volume of live cultures was transferred to the pad, sealed under a coverslip and transferred to the microscope for immediate visualization. A T*i* eclipse inverted research microscope with 100x/1.45 NA objective housed in a heated chamber, pre-heated to 30°C unless otherwise specified, was used to collect images.

23

509 Fluorescence images were captured using excitation and emission filter cubes for mVenus

510 (YFP), mCerulean (CFP), Hoechst 33258 (DAPI), and mCherry (Texas Red), ensuring that

511 fluorescence levels did not exceed the dynamic range of the sensor.

512      To visualize the chromosome, cultures of *Caulobacter* were fixed using a final

513 concentration of 4% formaldehyde for 5 min, following which DNA was stained for 25 min

514 using Hoechst 33258 at a final concentration of 2 μg/mL. Fixed cells were transferred to a 1%

515 agarose pad and visualized under the microscope as described above for live cells.

516

517 **Custom-built STED set-up and STED imaging**

518      The super-resolution imaging has been performed at a custom-built STED set-up. The

519 samples were fixed and adhered to slides as described by (Hiraga et al., 1998), and labelled

520 with an anti-GFP nanobody coupled to ATTO 594 (GFP-Booster_Atto594, ChromoTek). The

521 dye was excited with a 561 nm pulsed diode laser (PDL561, Abberior Instruments) and

522 subsequently depleted with a 775 nm pulsed laser (KATANA 08 HP, OneFive), both operating

523 at 40 MHz. The depletion beam was shaped to a donut in the focal plane by the use of a spatial

524 light modulator (LCOS-SLM X10468-02, Hamamatsu Photonics). The excitation laser and

525 depletion laser were coupled together and scanned over the sample using fast galvanometer

526 mirrors (galvanometer mirrors 6215H + servo driver 71215HHJ 671, Cambridge Technology).

527 The laser beams were focused onto the sample using a HC PL APO 100x/1.40 Oil STED White

528 objective lens (15506378, Leica Microsystems), through which also the fluorescence signal was

529 collected. After de-scanning and de-coupling of the fluorescence signal, it was put through a

530 confocal pinhole (1.28 Airy disk units) and detected through a bandpass filter (ET615/30m,

531 Chroma Technology) and a notch filter (ZET785NF, Chroma Technology) with a fiber-coupled

532 APD (SPCM-AQRH-14-FC, PerkinElmer).

533    The imaging was done with a 561 nm excitation laser power of 1.1-8.4 µW and a 775

534    nm depletion laser power of 132-158 mW, both measured at the first conjugate back focal plane

535    of the objective. The pixel size for all images was set to 25 nm. Each image was acquired by

536    adding up 10 line scans for each line, each with a pixel dwell time of 20 µs, resulting in a total

537    pixel dwell time of 200 µs.

538

539    **Aggregate size analysis**

540    The aggregate sizes were calculated from groups of fitted line profiles in the STED and

541    confocal images. Using Fiji (ImageJ), aggregates were picked out and line profiles were drawn

542    across them. The line profiles were extracted and fitted with a Lorentzian function, from which

543    the full width at half maximum was extracted as the aggregate size. The number of aggregates

544    used for each mean and standard deviation calculation was at least 60.

545

546    **Image and statistical analysis**

547    To prepare the appropriate image formats and to perform basic analyses such as foci

548    enumeration and generation of line profiles, the Fiji software package was used. Information

549    on the area of individual cells, their fluorescence intensity, as well as their corresponding

550    aggregate number and position in Figure 1D, E, 4, 5 and Supplemental Information Fig. 2 and

551    4 were gathered by analyzing binary masks of cells and aggregate foci using the ImageJ package

552    MicrobeJ (Ducret et al., 2016). The Oufti software package (Paintdakhi et al., 2016) was used

553    to generate data on population cell lengths in Figure 4F. To determine fluorescence intensity

554    per bacterial pixel shown in Figure 1I and 3C, the MATLAB package SuperSegger (Stylianidou

555    et al., 2016) was used to perform segmentation on images followed by calculation of total cell

556    area per image and bacterial fluorescence intensity per image. For the preparation of cell masks,

557    bacterial segmentation was performed on phase contrast images using SuperSegger and all

25

558    segmentation was manually checked before further analysis. Masks of the aggregate signal were

559    manually prepared by labeling corresponding areas. The colony kymograph in Figure 6B was

560    prepared based on cell and aggregate masks using SuperSegger to generate cell linking, cell

561    length, and aggregate position measurements. Aggregate inheritance and positional changes

562    after sequential divisions (Fig. 6, Supplemental Information Fig. 5, 6, 7) as well as the aggregate

563    life span (Fig. 4D, G, 5F, Supplemental Information Fig. 4B) were manually tracked. Data sets

564    generated through all image analysis programs were analyzed and visualized using MATLAB

565    and R software packages.

566

567    **Immunoblotting**

568    Cell pellets were collected following the indicated treatments and time points and

569    normalized by units $OD_{600}$ through dilution in Laemmli buffer. Diluted samples were boiled at

570    98°C for 10 min and loaded into Stain Free Tris-glycine gels (Bio-Rad) for separation by SDS-

571    PAGE and transfer to a nitrocellulose membrane as per manufacturer guidelines. Membranes

572    were blocked for 1 h in 5% skim milk powder in TBST and protein levels were detected using

573    either anti-DnaK antibody (Schramm et al., 2017) or the anti-GFP antibody (Thermo Fisher

574    Scientific, #A-11122). A secondary anti-rabbit HRP-conjugated antibody was used to detect

575    primary antibody binding, and SuperSignal Femto West (Thermo Fisher Scientific) used to

576    develop the membrane. Blots were scanned using a Chemidoc (Bio-Rad) system and signal

577    quantification was performed using the Image Lab software package (Bio-Rad).

578

579    **Aggregation assay**

580    The aggregation assay was performed as described in (Schramm et al., 2017). About 40

581    $OD_{600}$ units of cells with an $OD_{600}$ between 0.2-0.4 either grown at 30°C or heat stressed were

582    harvested. For the heat treatment an exponential overnight culture grown at 30°C was pelleted

26

583    (6000 g, 10 min, RT), resuspended in a flask containing 45°C pre-warmed medium and then

584    incubated shaking at the same temperature for 1 h. A portion of the aggregate fraction was

585    subjected to SDS-PAGE and the separated proteins were visualized by Coomassie staining

586    (Instant Blue Protein Stain, Expedeon).

587

588    **Proteomic analysis of protein aggregates**

589    For the identification of endogenous aggregating and aggregate associated proteins in

590    *Caulobacter crescentus* whole protein aggregate fractions were subjected to mass spectrometry

591    analysis. 0.1 µg horse cytochrome C were added to each sample to serve as internal protein

592    abundance standard. The mass spectrometry analysis of the samples was performed using an

593    Orbitrap Velos Pro mass spectrometer (Thermo Scientific). An Ultimate nanoRSLC-HPLC

594    system (Dionex), equipped with a custom 20 cm x 75 µm C18 RP column filled with 1.7 µm

595    beads was connected online to the mass spectrometer through a Proxeon nanospray source. 1-

596    15 µL of the tryptic digest (depending on sample concentration) were injected onto a C18 pre-

597    concentration column. Automated trapping and desalting of the sample was performed at a

598    flowrate of 6 µL/min using water/0.05% formic acid as solvent. Separation of the tryptic

599    peptides was achieved with the following gradient of water/0.05% formic acid (solvent A) and

600    80% acetonitrile/0.045% formic acid (solvent B) at a flow rate of 300 nL/min: holding 4% B

601    for five minutes, followed by a linear gradient to 45% B within 30 minutes and linear increase

602    to 95% solvent B in additional 5 minutes. The column was connected to a stainless steel

603    nanoemitter (Proxeon, Denmark) and the eluent was sprayed directly towards the heated

604    capillary of the mass spectrometer using a potential of 2300 V. A survey scan with a resolution

605    of 60000 within the Orbitrap mass analyzer was combined with at least three data-dependent

606    MS/MS scans with dynamic exclusion for 30 s either using CID with the linear ion-trap or using

607    HCD combined with orbitrap detection at a resolution of 7500. Data analysis was performed

608     using Proteome Discoverer (Thermo Scientific) with SEQUEST search engine using Uniprot

609     databases. The peptide peak areas of each protein in a sample were normalized to that of the

610     internal Cytochrome C standard. Proteins were considered to be specifically enriched in the

611     aggregate fraction if they were only detected in the heat-treated sample or more abundant than

612     in the control.

613

614     **Spot colony formation assays**

615          Cultures with an $OD_{600}$ between 0.1-0.4 were diluted to 0.05 after which a 1:10 serial

616     dilution was performed. 2 µL of each dilution were spotted on PYE agar plates.

## **Acknowledgements**

# References

Aaron M, Charbon G, Lam H, Schwarz H, Vollmer W, Jacobs-Wagner C. 2007. The tubulin homologue FtsZ contributes to cell elongation by guiding cell wall precursor synthesis in Caulobacter crescentus. *Mol Microbiol* **64**:938–952. doi:10.1111/j.1365-2958.2007.05720.x

Ackermann M, Stearns SC, Jenal U. 2003. Senescence in a bacterium with asymmetric division. *Science* **300**:1920. doi:10.1126/science.1083532

Aguilaniu H, Gustafsson L, Rigoulet M, Nyström T. 2003. Asymmetric inheritance of oxidatively damaged proteins during cytokinesis. *Science* **299**:1751–1753. doi:10.1126/science.1080418

Baldini RL, Avedissian M, Gomes SL. 1998. The CIRCE element and its putative repressor control cell cycle expression of the Caulobacter crescentus groESL operon. *J Bacteriol* **180**:1632–1641.

Barthel TK, Zhang J, Walker GC. 2001. ATPase-Defective Derivatives of Escherichia coli DnaK That Behave Differently with Respect to ATP-Induced Conformational Change and Peptide Release. *J Bacteriol* **183**:5482–5490. doi:10.1128/JB.183.19.5482-5490.2001

Bergmiller T, Andersson AMC, Tomasek K, Balleza E, Kiviet DJ, Hauschild R, Tkačik G, Guet CC. 2017. Biased partitioning of the multidrug efflux pump AcrAB-TolC underlies long-lived phenotypic heterogeneity. *Science* **356**:311–315. doi:10.1126/science.aaf4762

Chen K, Gao Y, Mih N, O'Brien EJ, Yang L, Palsson BO. 2017. Thermosensitivity of growth is determined by chaperone-mediated proteome reallocation. *Proc Natl Acad Sci* **114**:11548–11553. doi:10.1073/pnas.1705524114

647    Coelho M, Lade SJ, Alberti S, Gross T, Tolić IM. 2014. Fusion of Protein Aggregates

648        Facilitates Asymmetric Damage Segregation. *PLoS Biol* **12**:e1001886.

649        doi:10.1371/journal.pbio.1001886

650    Coquel A-S, Jacob J-P, Primet M, Demarez A, Dimiccoli M, Julou T, Moisan L, Lindner AB,

651        Berry H. 2013. Localization of protein aggregation in Escherichia coli is governed by

652        diffusion and nucleoid macromolecular crowding effect. *PLoS Comput Biol*

653        **9**:e1003038. doi:10.1371/journal.pcbi.1003038

654    Curtis PD, Brun YV. 2010. Getting in the loop: regulation of development in Caulobacter

655        crescentus. *Microbiol Mol Biol Rev MMBR* **74**:13–41. doi:10.1128/MMBR.00040-09

656    Da Silva ACA, Simão RCG, Susin MF, Baldini RL, Avedissian M, Gomes SL. 2003.

657        Downregulation of the heat shock response is independent of DnaK and σ32 levels in

658        Caulobacter crescentus: Heat shock response regulation in Caulobacter. *Mol Microbiol*

659        **49**:541–553. doi:10.1046/j.1365-2958.2003.03581.x

660    Ducret A, Quardokus EM, Brun YV. 2016. MicrobeJ, a tool for high throughput bacterial cell

661        detection and quantitative analysis. *Nat Microbiol* **1**:16077.

662        doi:10.1038/nmicrobiol.2016.77

663    Erjavec N, Larsson L, Grantham J, Nyström T. 2007. Accelerated aging and failure to

664        segregate damaged proteins in Sir2 mutants can be suppressed by overproducing the

665        protein aggregation-remodeling factor Hsp104p. *Genes Dev* **21**:2410–2421.

666        doi:10.1101/gad.439307

667    Fay A, Glickman MS. 2014. An essential nonredundant role for mycobacterial DnaK in

668        native protein folding. *PLoS Genet* **10**:e1004516. doi:10.1371/journal.pgen.1004516

669    Glover JR, Lindquist S. 1998. Hsp104, Hsp70, and Hsp40. *Cell* **94**:73–82.

670        doi:10.1016/S0092-8674(00)81223-4

31

671    Goloubinoff P, Mogk A, Zvi APB, Tomoyasu T, Bukau B. 1999. Sequential mechanism of

672          solubilization and refolding of stable protein aggregates by a bichaperone network.

673          *Proc Natl Acad Sci* **96**:13732–13737. doi:10.1073/pnas.96.24.13732

674    Govers SK, Dutré P, Aertsen A. 2014. In vivo disassembly and reassembly of protein

675          aggregates in Escherichia coli. *J Bacteriol* **196**:2325–2332. doi:10.1128/JB.01549-14

676    Govers SK, Mortier J, Adam A, Aertsen A. 2018. Protein aggregates encode epigenetic

677          memory of stressful encounters in individual Escherichia coli cells. *PLoS Biol*

678          **16**:e2003853. doi:10.1371/journal.pbio.2003853

679    Grousl T, Ungelenk S, Miller S, Ho C-T, Khokhrina M, Mayer MP, Bukau B, Mogk A. 2018.

680          A prion-like domain in Hsp42 drives chaperone-facilitated aggregation of misfolded

681          proteins. *J Cell Biol* **217**:1269–1285. doi:10.1083/jcb.201708116

682    Hartl FU, Bracher A, Hayer-Hartl M. 2011. Molecular chaperones in protein folding and

683          proteostasis. *Nature* **475**:324–332. doi:10.1038/nature10317

684    Heck JW, Cheung SK, Hampton RY. 2010. Cytoplasmic protein quality control degradation

685          mediated by parallel actions of the E3 ubiquitin ligases Ubr1 and San1. *Proc Natl*

686          *Acad Sci U S A* **107**:1106–1111. doi:10.1073/pnas.0910591107

687    Heinrich K, Sobetzko P, Jonas K. 2016. A Kinase-Phosphatase Switch Transduces

688          Environmental Information into a Bacterial Cell Cycle Circuit. *PLoS Genet*

689          **12**:e1006522. doi:10.1371/journal.pgen.1006522

690    Henry JT, Crosson S. 2013. Chromosome replication and segregation govern the biogenesis

691          and inheritance of inorganic polyphosphate granules. *Mol Biol Cell* **24**:3177–3186.

692          doi:10.1091/mbc.E13-04-0182

693    Higuchi R, Vevea JD, Swayne TC, Chojnowski R, Hill V, Boldogh IR, Pon LA. 2013. Actin

694          dynamics affect mitochondrial quality control and aging in budding yeast. *Curr Biol*

695          *CB* **23**:2417–2422. doi:10.1016/j.cub.2013.10.022

696    Hill SM, Hao X, Grönvall J, Spikings-Nordby S, Widlund PO, Amen T, Jörhov A, Josefson

697          R, Kaganovich D, Liu B, Nyström T. 2016. Asymmetric Inheritance of Aggregated

698          Proteins and Age Reset in Yeast Are Regulated by Vac17-Dependent Vacuolar

699          Functions. *Cell Rep* **16**:826–838. doi:10.1016/j.celrep.2016.06.016

700    Hill SM, Hao X, Liu B, Nyström T. 2014. Life-span extension by a metacaspase in the yeast

701          Saccharomyces cerevisiae. *Science* **344**:1389–1392. doi:10.1126/science.1252634

702    Hiraga S, Ichinose C, Niki H, Yamazoe M. 1998. Cell cycle-dependent duplication and

703          bidirectional migration of SeqA-associated DNA-protein complexes in E. coli. *Mol*

704          *Cell* **1**:381–387.

705    Jonas K, Liu J, Chien P, Laub MT. 2013. Proteotoxic stress induces a cell-cycle arrest by

706          stimulating Lon to degrade the replication initiator DnaA. *Cell* **154**:623–636.

707          doi:10.1016/j.cell.2013.06.034

708    Kanemori M, Nishihara K, Yanagi H, Yura T. 1997. Synergistic roles of HslVU and other

709          ATP-dependent proteases in controlling in vivo turnover of sigma32 and abnormal

710          proteins in Escherichia coli. *J Bacteriol* **179**:7219–7225.

711    Kohanski MA, Dwyer DJ, Wierzbowski J, Cottarel G, Collins JJ. 2008. Mistranslation of

712          Membrane Proteins and Two-Component System Activation Trigger Antibiotic-

713          Mediated Cell Death. *Cell* **135**:679–690. doi:10.1016/j.cell.2008.09.038

714    Kumar M, Sourjik V. 2012. Physical map and dynamics of the chaperone network in

715          Escherichia coli. *Mol Microbiol* **84**:736–747. doi:10.1111/j.1365-2958.2012.08054.x

716    Lambert A, Vanhecke A, Archetti A, Holden S, Schaber F, Pincus Z, Laub MT, Goley E,

717          Manley S. 2018. Constriction rate modulation can drive cell size control and

718          homeostasis in C. crescentus. *iScience*. doi:10.1016/j.isci.2018.05.020

719    Lindner AB, Madden R, Demarez A, Stewart EJ, Taddei F. 2008. Asymmetric segregation of

720        protein aggregates is associated with cellular aging and rejuvenation. *Proc Natl Acad*

721        *Sci U S A* **105**:3076–3081. doi:10.1073/pnas.0708931105

722    Mogk A, Bukau B, Kampinga HH. 2018. Cellular Handling of Protein Aggregates by

723        Disaggregation Machines. *Mol Cell* **69**:214–226. doi:10.1016/j.molcel.2018.01.004

724    Mogk A, Deuerling E, Vorderwülbecke S, Vierling E, Bukau B. 2003a. Small heat shock

725        proteins, ClpB and the DnaK system form a functional triade in reversing protein

726        aggregation. *Mol Microbiol* **50**:585–595.

727    Mogk A, Schlieker C, Friedrich KL, Schönfeld H-J, Vierling E, Bukau B. 2003b. Refolding

728        of Substrates Bound to Small Hsps Relies on a Disaggregation Reaction Mediated

729        Most Efficiently by ClpB/DnaK. *J Biol Chem* **278**:31033–31042.

730        doi:10.1074/jbc.M303587200

731    Nyström T, Liu B. 2014. The mystery of aging and rejuvenation - a budding topic. *Curr Opin*

732        *Microbiol* **18**:61–67. doi:10.1016/j.mib.2014.02.003

733    Paintdakhi A, Parry B, Campos M, Irnov I, Elf J, Surovtsev I, Jacobs-Wagner C. 2016. Oufti:

734        an integrated software package for high-accuracy, high-throughput quantitative

735        microscopy analysis. *Mol Microbiol* **99**:767–777. doi:10.1111/mmi.13264

736    Rosen R, Biran D, Gur E, Becher D, Hecker M, Ron EZ. 2002. Protein aggregation in

737        Escherichia coli: role of proteases. *FEMS Microbiol Lett* **207**:9–12.

738    Saarikangas J, Barral Y. 2015. Protein aggregates are associated with replicative aging

739        without compromising protein quality control. *eLife* **4**. doi:10.7554/eLife.06197

740    Santra M, Dill KA, de Graff AMR. 2018. How Do Chaperones Protect a Cell's Proteins from

741        Oxidative Damage? *Cell Syst*. doi:10.1016/j.cels.2018.05.001

742    Santra M, Farrell DW, Dill KA. 2017. Bacterial proteostasis balances energy and chaperone

743        utilization efficiently. *Proc Natl Acad Sci* **114**:E2654–E2661.

744        doi:10.1073/pnas.1620646114

745    Schramm FD, Heinrich K, Thüring M, Bernhardt J, Jonas K. 2017. An essential regulatory

746        function of the DnaK chaperone dictates the decision between proliferation and

747        maintenance in Caulobacter crescentus. *PLOS Genet* **13**:e1007148.

748        doi:10.1371/journal.pgen.1007148

749    Shapiro L, McAdams HH, Losick R. 2002. Generating and exploiting polarity in bacteria.

750        *Science* **298**:1942–1946. doi:10.1126/science.1072163

751    Shcheprova Z, Baldi S, Frei SB, Gonnet G, Barral Y. 2008. A mechanism for asymmetric

752        segregation of age during yeast budding. *Nature* **454**:728–734.

753        doi:10.1038/nature07212

754    Simão RCG, Susin MF, Alvarez-Martinez CE, Gomes SL. 2005. Cells lacking ClpB display a

755        prolonged shutoff phase of the heat shock response in *Caulobacter crescentus*:

756        *Caulobacter crescentus* ClpB. *Mol Microbiol* **57**:592–603. doi:10.1111/j.1365-

757        2958.2005.04713.x

758    Specht S, Miller SBM, Mogk A, Bukau B. 2011. Hsp42 is required for sequestration of

759        protein aggregates into deposition sites in Saccharomyces cerevisiae. *J Cell Biol*

760        **195**:617–629. doi:10.1083/jcb.201106037

761    Spokoini R, Moldavski O, Nahmias Y, England JL, Schuldiner M, Kaganovich D. 2012.

762        Confinement to organelle-associated inclusion structures mediates asymmetric

763        inheritance of aggregated protein in budding yeast. *Cell Rep* **2**:738–747.

764        doi:10.1016/j.celrep.2012.08.024

765    Strozecka J, Chrusciel E, Gorna E, Szymanska A, Zietkiewicz S, Liberek K. 2012.

766        Importance of N- and C-terminal Regions of IbpA, Escherichia coli Small Heat Shock

767    Protein, for Chaperone Function and Oligomerization. *J Biol Chem* **287**:2843–2853.

768    doi:10.1074/jbc.M111.273847

769 Stylianidou S, Brennan C, Nissen SB, Kuwada NJ, Wiggins PA. 2016. SuperSegger: robust

770    image segmentation, analysis and lineage tracking of bacterial cells. *Mol Microbiol*

771    **102**:690–700. doi:10.1111/mmi.13486

772 Tomoyasu T, Mogk A, Langen H, Goloubinoff P, Bukau B. 2001. Genetic dissection of the

773    roles of chaperones and proteases in protein folding and degradation in the Escherichia

774    coli cytosol. *Mol Microbiol* **40**:397–413.

775 Tyedmers J, Mogk A, Bukau B. 2010. Cellular strategies for controlling protein aggregation.

776    *Nat Rev Mol Cell Biol* **11**:777–788. doi:10.1038/nrm2993

777 Ungelenk S, Moayed F, Ho C-T, Grousl T, Scharf A, Mashaghi A, Tans S, Mayer MP, Mogk

778    A, Bukau B. 2016. Small heat shock proteins sequester misfolding proteins in near-

779    native conformation for cellular protection and efficient refolding. *Nat Commun*

780    **7**:13673. doi:10.1038/ncomms13673

781 Van Melderen L, Aertsen A. 2009. Regulation and quality control by Lon-dependent

782    proteolysis. *Res Microbiol* **160**:645–651. doi:10.1016/j.resmic.2009.08.021

783 Vaubourgeix J, Lin G, Dhar N, Chenouard N, Jiang X, Botella H, Lupoli T, Mariani O, Yang

784    G, Ouerfelli O, Unser M, Schnappinger D, McKinney J, Nathan C. 2015. Stressed

785    mycobacteria use the chaperone ClpB to sequester irreversibly oxidized proteins

786    asymmetrically within and between cells. *Cell Host Microbe* **17**:178–190.

787    doi:10.1016/j.chom.2014.12.008

788 Vedel S, Nunns H, Košmrlj A, Semsey S, Trusina A. 2016. Asymmetric Damage Segregation

789    Constitutes an Emergent Population-Level Stress Response. *Cell Syst* **3**:187–198.

790    doi:10.1016/j.cels.2016.06.008

791    Wallace EWJ, Kear-Scott JL, Pilipenko EV, Schwartz MH, Laskowski PR, Rojek AE,

792         Katanski CD, Riback JA, Dion MF, Franks AM, Airoldi EM, Pan T, Budnik BA,

793         Drummond DA. 2015. Reversible, Specific, Active Aggregates of Endogenous

794         Proteins Assemble upon Heat Stress. *Cell* **162**:1286–1298.

795         doi:10.1016/j.cell.2015.08.041

796    Winkler J, Seybert A, König L, Pruggnaller S, Haselmann U, Sourjik V, Weiss M, Frangakis

797         AS, Mogk A, Bukau B. 2010. Quantitative and spatio-temporal features of protein

798         aggregation in Escherichia coli and consequences on protein quality control and

799         cellular ageing. *EMBO J* **29**:910–923. doi:10.1038/emboj.2009.412

800    Wu W, Xing L, Zhou B, Lin Z. 2011. Active protein aggregates induced by terminally

801         attached self-assembling peptide ELK16 in Escherichia coli. *Microb Cell Factories*

802         **10**:9. doi:10.1186/1475-2859-10-9

803    Zhou C, Slaughter BD, Unruh JR, Eldakak A, Rubinstein B, Li R. 2011. Motility and

804         segregation of Hsp104-associated protein aggregates in budding yeast. *Cell* **147**:1186–

805         1196. doi:10.1016/j.cell.2011.11.002

806

807 **Figures**
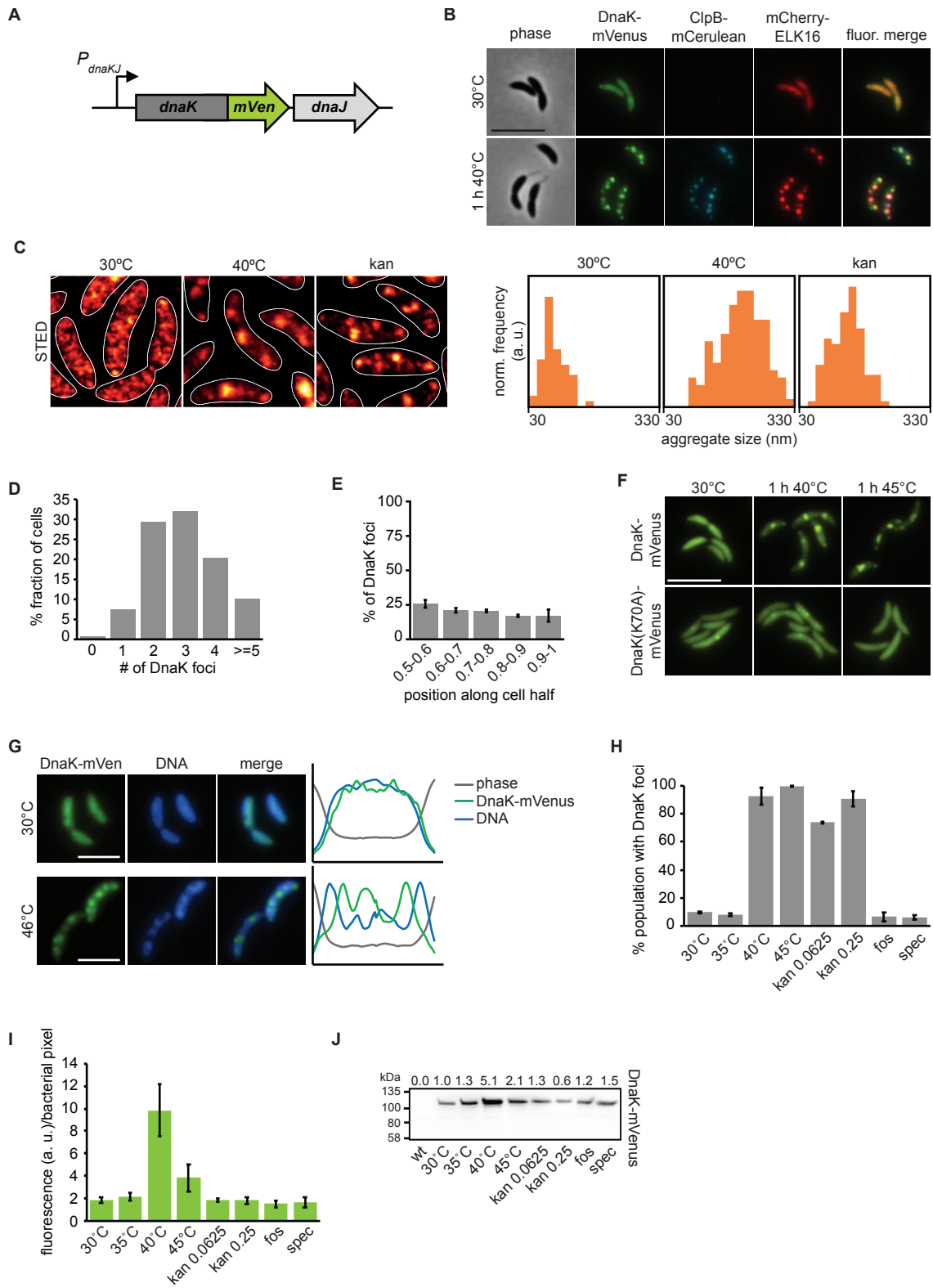


808

809

810   **Figure 1. Stress induces relocalization of chaperone machinery to foci of protein**

811   **aggregation.**

812   (A) Fluorescent fusions to proteins at their native locus are used to visualize the location of

813   chaperones. (B) Microscopy of DnaK-mVenus, ClpB-mCerulean, and mCherry-ELK16

814   expressed at 30°C and after 1 h of heat shock at 40°C. (C) Representative images demonstrating

815   DnaK-mVenus localization at super-resolution with STED imaging following incubation at

816   30°C, 1 h at 40°C, and after 1 h treatment with 0.25 µg/ml kanamycin. STED images are

817   smoothed and cell outlines are shown in white. The histograms show the distribution of

818   aggregate sizes, with all histograms showing the size range of 30-330 nm, and a bin width of

819   20 nm. Histograms show the size distribution of at least 60 aggregates. (D) Quantification of

820   the number of aggregates per cell and (E) graph illustrating the position of the aggregates along

821   five bins from midcell (0.5) to the cell pole (1) in cells exposed to 1 h of 40°C in liquid culture.

822   Quantifications in (D) and (E) show the means of biological triplicates for which at least 196

823   cells and 685 aggregates each were analyzed, respectively. Error bars represent standard

824   deviations. (F) Microscopy comparing localization of DnaK-mVenus with DnaK70A-mVenus

825   at 30°C and after 1 h at 40°C. (G) Fluorescence microscopy demonstrating localization of

826   DnaK-mVenus and the chromosome, stained with Hoechst 33258, after incubation at 30°C and

827   46°C. Line profiles (right) demonstrate fluorescence or phase contrast signal over the length of

828   a representative cell from each treatment group. Signals are plotted as the percentage of the

829   maximum value. Scale bar is 2.5 µm. (H) DnaK-mVenus foci formation in response to different

830   stress conditions. Cultures of the DnaK-mVenus strain were exposed to the indicated

831   temperature or treated with 0.0625 µg/ml or 0.25 µg/ml kanamycin, 20 µg/ml fosfomycin (fos),

832   or 100 µg/ml spectinomycin (spec) for 1 h followed by visualization and quantification of the

833   number of cells with DnaK-mVenus foci. Quantifications show the means of biological

834   duplicates where 300 cells each were analyzed. Error bars represent standard deviation. (I)

835    Quantification of DnaK-mVenus fluorescence intensity under different stress conditions.

836    Cultures of the DnaK-mVenus strain were treated as in (H) followed by imaging and

837    quantification of fluorescence intensity per bacterial pixel. Quantifications show the means of

838    biological duplicates where at least 339 total cells each were analyzed from at least 10

839    independent images. (J) Quantification of protein levels of DnaK-mVenus under the conditions

840    described in (H) and (I) by western blot. Band intensities are shown as average of two replicates

841    above the western blot image.

842
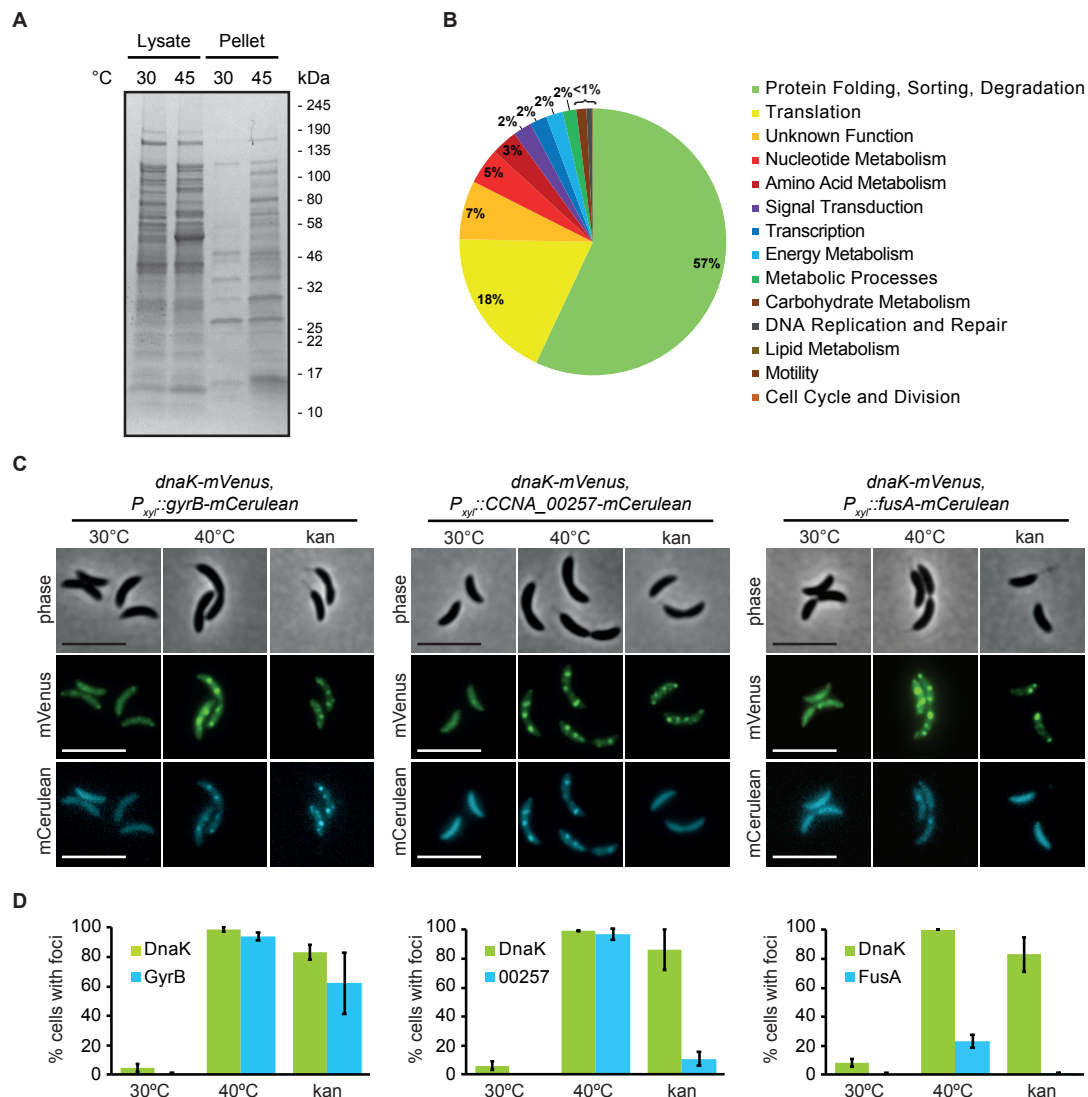
**Figure 2. Proteins governing diverse processes aggregate in *C. crescentus*.**

(A) Coomassie stained protein gel of soluble and detergent-resistant aggregated fractions following heat stress. Wild type cultures at 30°C and 1 h at 45°C were collected and soluble and insoluble fractions were separated by lysis and centrifugation. (B) Abundance of aggregate-enriched proteins sorted by functional category. Functional categories were assigned to proteins identified in (A) according to KEGG gene ontology, and the enrichment of aggregation-prone proteins belonging to each category was determined to obtain relative abundance. (C) Localization pattern of the aggregation-prone proteins GyrB, CCNA_00257, and FusA at 30°C and 40°C. Expression of the fusion proteins was induced for 3 h at 30°C, followed by 1 h exposure to 40°C or 0.25 μM kanamycin. Scale bar is 5 μm. (D). Quantification of stress

854     induced relocalization of endogenous aggregating proteins and DnaK-mVenus shown in (C).

855     Quantifications show the means of biological duplicates where at least 152 cells each were

856     analyzed. Error bars represent standard deviation.

857
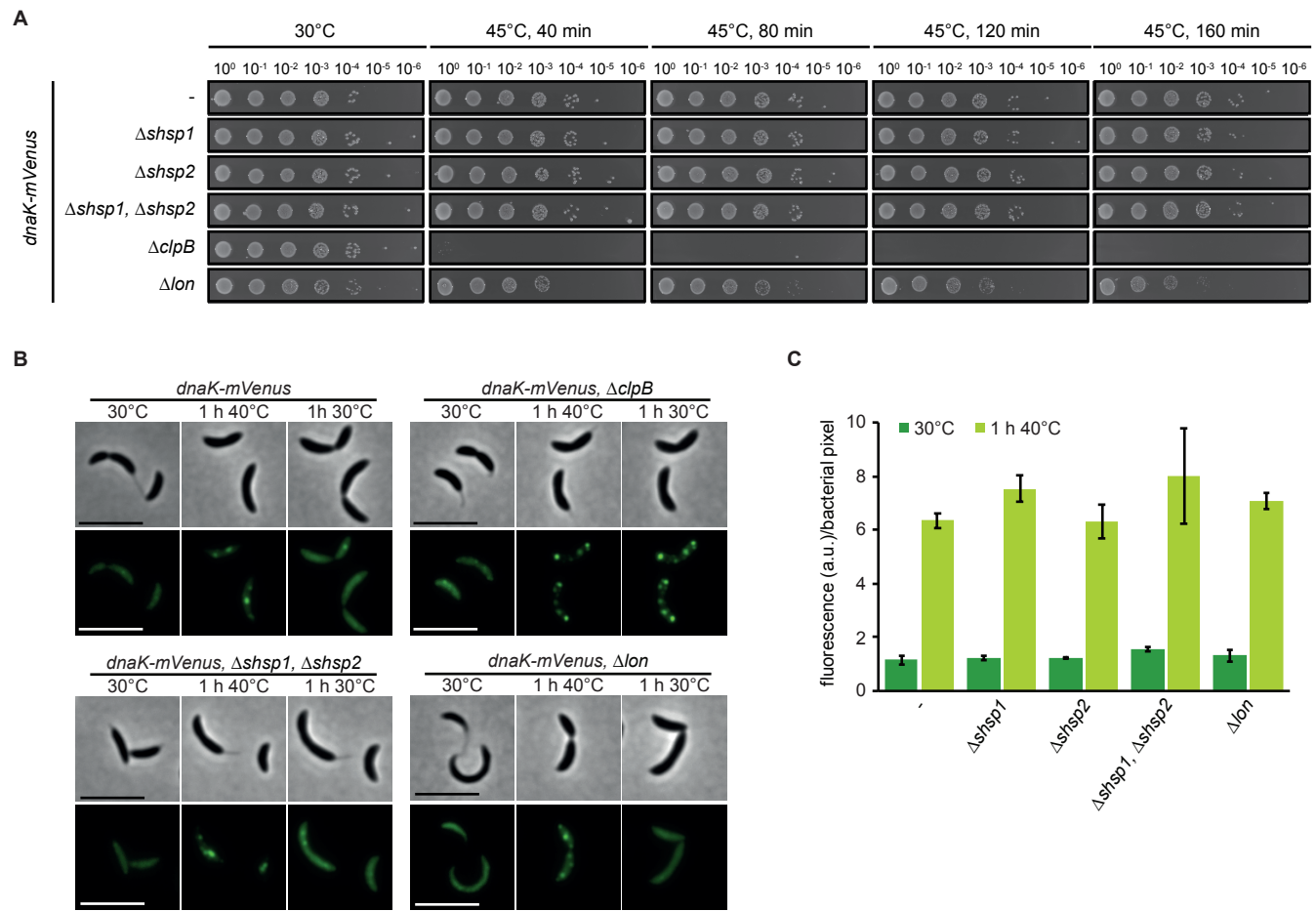
**Figure 3. Contribution of chaperones and proteases to stress resistance**

(A) Spot assays comparing colony formation of wild type, the *dnaK::dnaK-mVenus* strain and its derivative strains harboring chaperone and protease knockouts grown at 30°C without stress treatment or after 40, 80, 120 or 160 minutes of incubation at 45°C. (B) DnaK-mVenus localization in the same strains as in (A) grown at 30°C or after heat shock in liquid culture at 40°C for one hour (1 h 40°C panels). After 40°C heat shock, cells were permitted to recover at 30°C for one hour (1 h 30°C panels), during which aggregate dissolution was monitored by time lapse microscopy. (C) Absolute measurements of DnaK-mVenus fluorescence during growth at 30°C and after one hour heat shock at 40°C. Quantifications show the means of biological duplicates where at least 409 cells each were analyzed from 10 independent images.
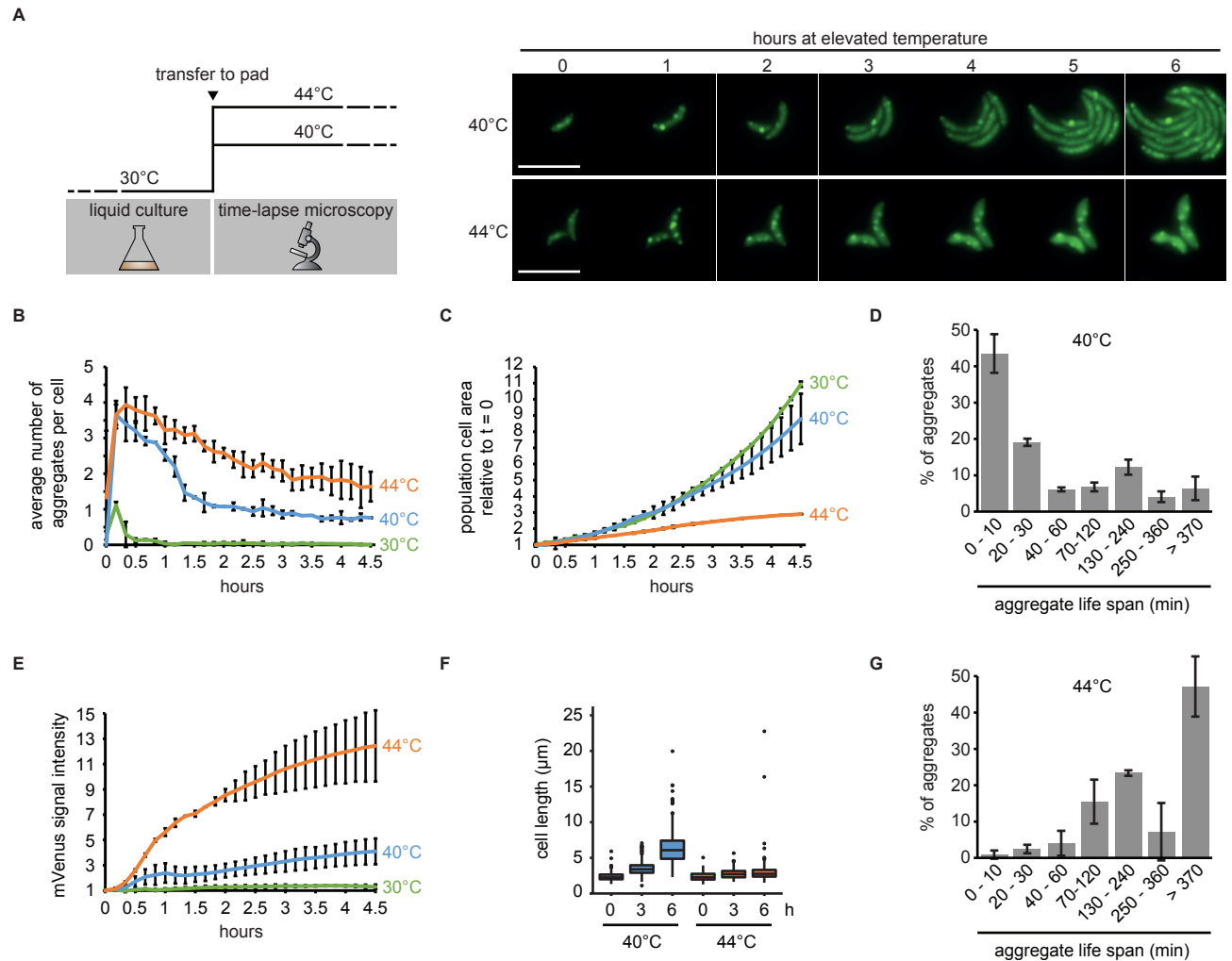
870

871 **Figure 4. Growth and protein aggregation dynamics during sustained heat stress.**

872 (A) Schematic of upshift experiments (left), and representative images following upshift to

873 40°C or 44°C over a six hour period. (B) Quantifications of fluorescence time-lapse microscopy

874 images showing the average number of aggregates per cell over time in cell populations

875 continuously grown at 30, 40 and 44°C. Note that after transfer to 30°C a minor fraction of dim

876 and short-lived DnaK-mVenus foci formed. (C) Total cell area increase during exposure to 30,

877 40, or 44°C relative to the first time point (t=0). Quantifications in (B, C) show the means of

878 biological triplicates for which at least 8 microcolonies each were analyzed. Error bars represent

879 standard deviations. (D) Quantification of aggregate life span in cells continuously exposed to

880 40°C. Aggregates present or emerging in the first 300 min of a fluorescence time-lapse movie

44

881    were tracked until 400 min. Images were acquired every 10 min. Quantifications show the

882    means of biological triplicates for which at least five microcolonies and 89 aggregates each

883    were analyzed. Error bars represent standard deviations. (E) DnaK-mVenus fluorescence

884    intensity per bacterial pixel over time in cells grown at 30, 40, or 44°C normalized to the first

885    time point (t=0). The same cells as in (B, C) were quantified. (F) Quantification of population

886    cell lengths after 0, 3, and 6 hours continuous exposure to 40, or 44°C. The cell lengths of two

887    biological replicates were pooled and populations representing at least 504 measurements are

888    shown. (G) Quantification of aggregate life span in cells continuously exposed to 44°C.

889    Aggregates present at 0 min were tracked until 480 min (new aggregates did not arise). Images

890    were acquired every 10 min. Quantifications show the means of biological duplicates for which

891    at least 14 microcolonies and 63 aggregates each were analyzed. Error bars represent standard

892    deviations.

893
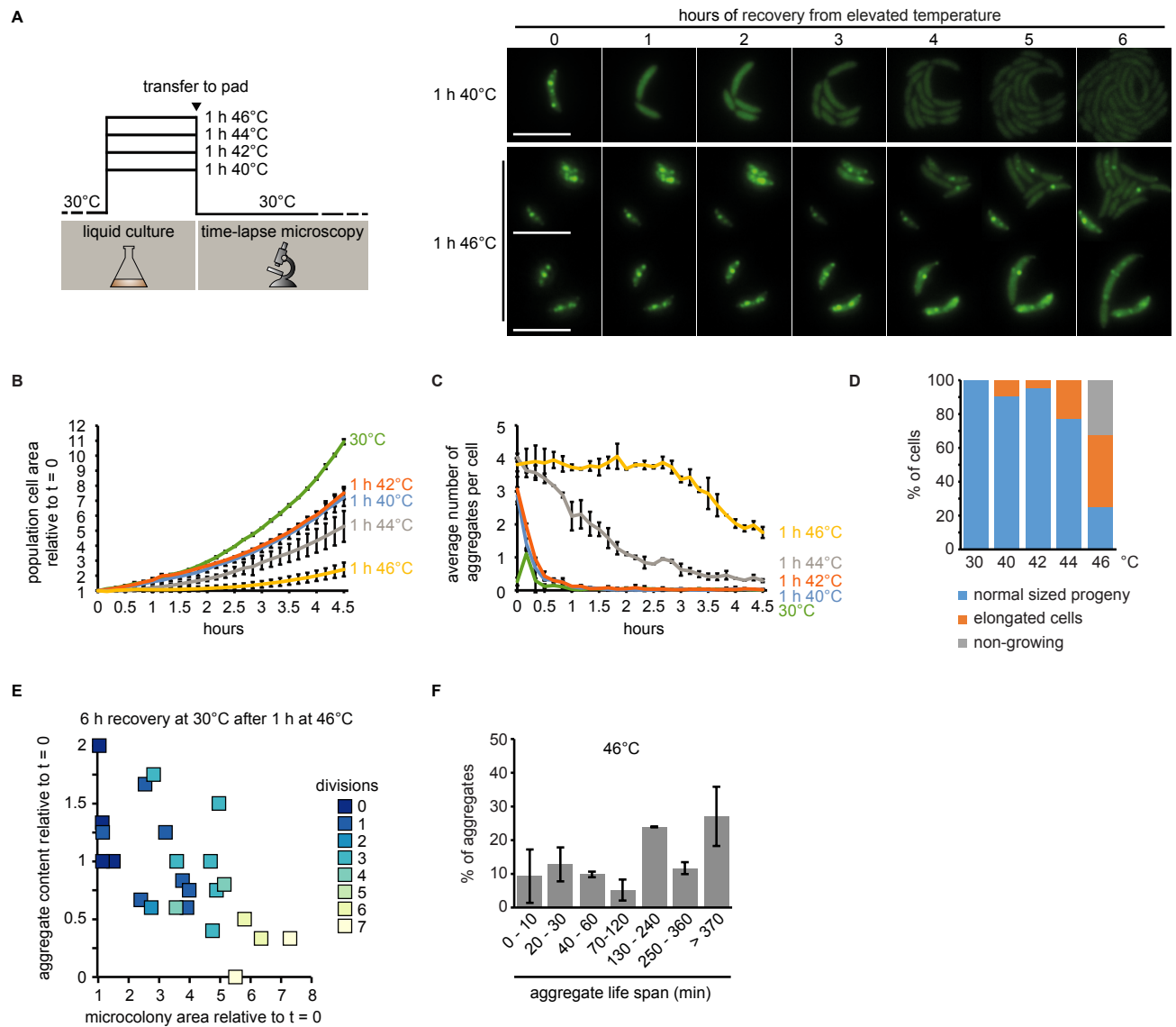
**Figure 5. Growth and aggregate clearance following stress recovery.**

(A) Schematic of recovery experiments (left) and representative images from recovery after exposure to 40°C and 46°C for one hour. Two panels are shown for the 46°C condition to represent the diversity of cell fates after stress release. (B) Quantifications of fluorescence time-lapse microscopy showing the average number of aggregates per cell in cell populations recovering from one hour of exposure to 40, 42, 44 and 46°C. (C) Total cell area increase over time after release from one hour exposure to 40, 42, 44 and 46°C relative to the first time point (t=0). Quantifications in (B, C) show the means of biological duplicates for which at least 9 microcolonies each were analyzed. The data on cells continuously grown at 30°C are the same

904 as in Fig. 4. Error bars represent standard deviations. (D) Quantification of cell fates during

905 continuous growth at 30°C, or recovery at 30°C after 1 h of exposure to 40, 42, 44 and 46°C.

906 Quantifications are based on tracking at least 21 cells/microcolonies per duplicate condition.

907 Cell/microcolony properties were quantified when the average total area of the population

908 increased to four times the initial area. Growing cells/microcolonies were defined as those that

909 at least doubled in area. Elongated cells or microcolonies containing those were considered as

910 such when the average cell length in the microcolony was at least 1.5 times higher than the

911 average cell length of a population grown to four times the cell area under continuous 30°C

912 conditions. (E) Scatter plot representing relative area increase, relative aggregate number

913 normalized to the amount present at stress release and the number of divisions of 24 cells and

914 their potential progeny after six hours (the time at which the average area of the population has

915 quadrupled) at 30°C on pad after release from one hour of exposure to 46°C. (F) Quantification

916 of aggregate life span in cells recovering from exposure to 1 h 46°C forming microcolonies of

917 mostly normally sized cells (D). Aggregates present or emerging in the first 400 min of a

918 fluorescence time-lapse movie were tracked until 500 min. Images were acquired every 10 min.

919 Quantifications show the means of biological duplicates for which at least eight microcolonies

920 and 54 aggregates each were analyzed. Error bars represent standard deviations.

921
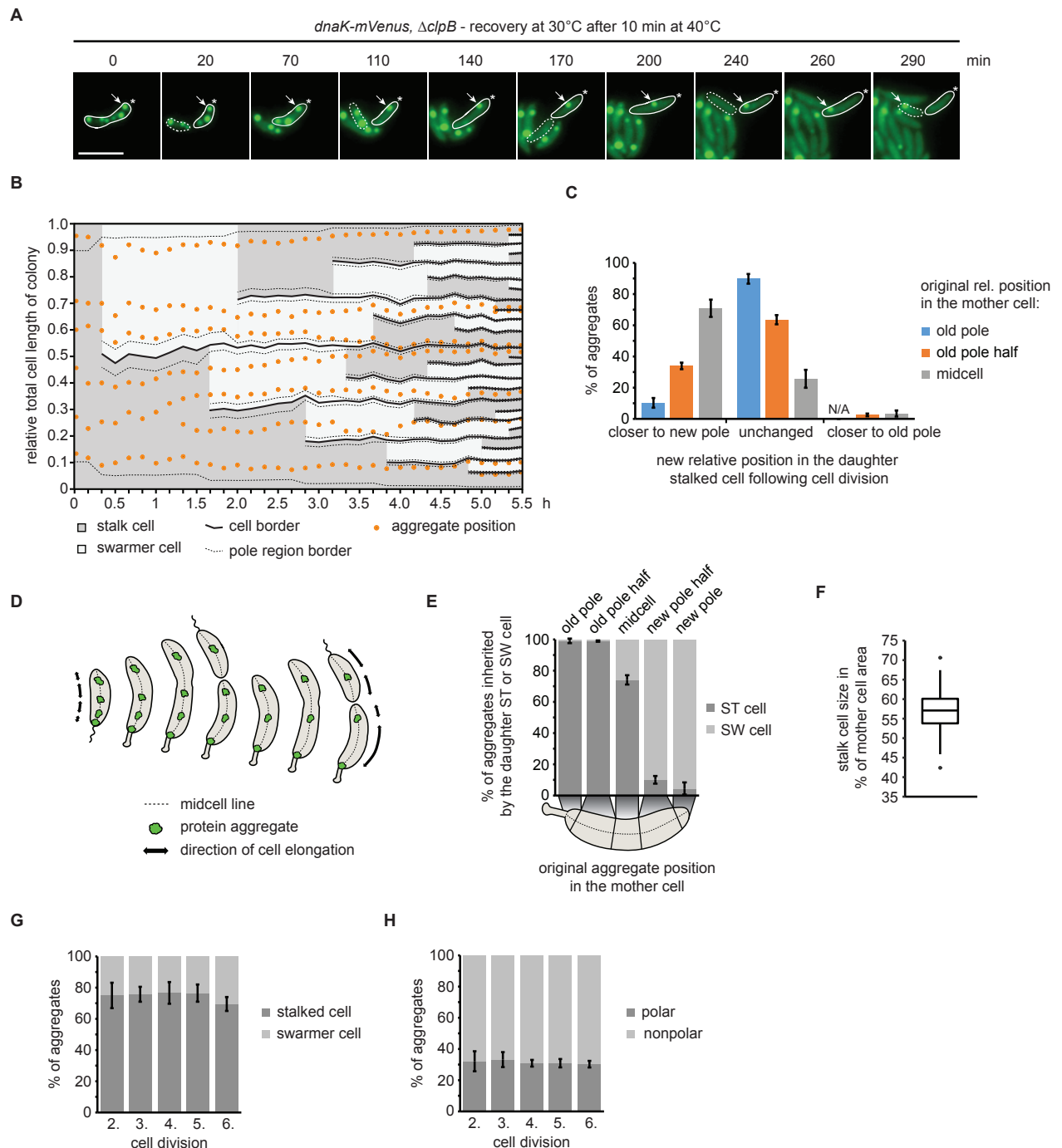
**Figure 6. Inheritance of persistent protein aggregates in the ΔclpB background recovering from heat stress.** (A) Representative fluorescence time-lapse images of the recovery at 30°C after exposure to 40°C for 10 min pointing out the inheritance of an aggregate originally localized in the old pole cell half after stress exposure (arrow). The star represents the location of the old pole. The stalked cell is outlined by a solid and the swarmer cell by a dashed line. (B) Kymograph normalized to the summed length of all descendants, showing

929    relative aggregate localization and cell polarity changes during microcolony growth. Cell

930    borders arising through cell divisions are represented by solid lines while the 10% of the cell

931    length defined as the pole region is indicated by dashed lines. (C) Quantitative data showing

932    how aggregates change their relative cellular position in the daughter stalked cell as a

933    consequence of cell division. (D) Schematic model of how cell growth contributes to the

934    movement of stationary aggregates. (E) Proportion of aggregates inherited by either a swarmer

935    or a stalked cell as function of their cellular position in the mother cell. (F) Quantification of

936    the amount of the mother cell area inherited by the daughter stalked cell after a division event.

937    Quantification based on 160 division events occurring in the third and fourth generation of 33

938    microcolonies. (G) Percentage of aggregates inherited by the stalked or the swarmer daughter

939    cell after the second to the sixth division. (H) Localization of aggregates tracked from the

940    second to the sixth division. Aggregate position quantifications in (C, E, G and H) resulted from

941    tracking the same population of aggregates from the second to the sixth division.

942    Quantifications are based on biological triplicates for which at least 94 aggregates in at least 20

943    microcolonies each were tracked. For the quantifications in (C) and (E) the aggregate positional

944    changes after each division were binned leading to at least 376 aggregate positional changes

945    tracked per replicate. Error bars represent standard deviations.

1    **Supporting Information**

2

3    **Growth-driven displacement of protein aggregates along the cell length**

4    **ensures partitioning to both daughter cells in Caulobacter crescentus**

5    Frederic D. Schramm*, Kristen Schroeder*, Jonatan Alvelid, Ilaria Testa and Kristina Jonas

6    * Equal contribution

7

8    **Content**

9    **Supporting Information Figure 1.** Viability and functionality of the fluorescent reporters used

10    in this study.

11    **Supporting Information Figure 2.** Δ*clpB* cells recovering from mild heat stress do not

12    dissolve aggregates.

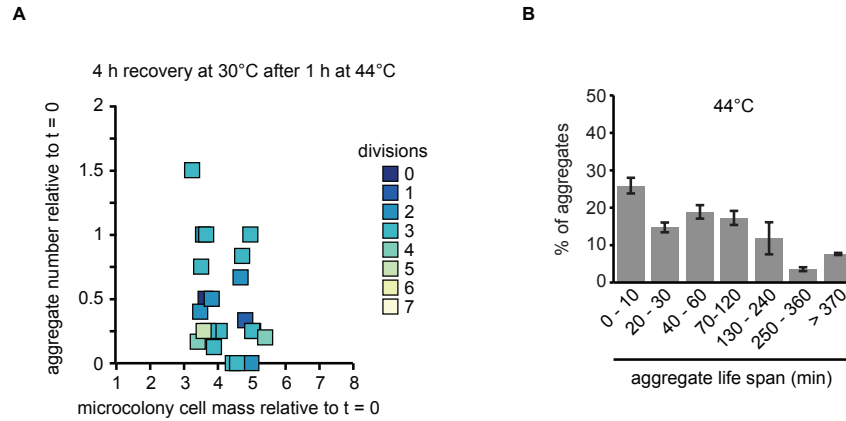13    **Supporting Information Figure 3.** Representative time courses of cells continuously growing

14    at 30°C or recovering from elevated temperature.

15    **Supporting Information Figure 4.** Growth and aggregate clearance in cells recovering from

16    1 h of exposure to 44°C.

17    **Supporting Information Figure 5.** Schematic table summarizing how positional changes after

18    cell divisions ranked by the position in the mother cell were quantified.

19    **Supporting Information Figure 6.** Inheritance of persistent protein aggregates in DnaK-

20    mVenus cells continuously exposed to 40°C.

21    **Supporting Information Figure 7.** Inheritance of persistent protein aggregates in DnaK-

22    mVenus cells continuously exposed to 44°C.

23    **Supporting Information Text 1**

24    **Supporting Information References**

25
26

27    **Additional Supporting Information:**

28    **Supporting Information Table 1.** Strains, plasmids and primers used in this study

29    **Supporting Information Table 2.** Proteins enriched in the aggregated fraction in *C. crescentus*

30    following exposure to 45°C

31    **Supporting Information Movie 1.** Time lapse microscopy of DnaK-mVenus upshift to 40°C

32
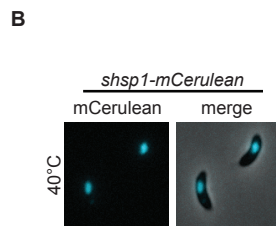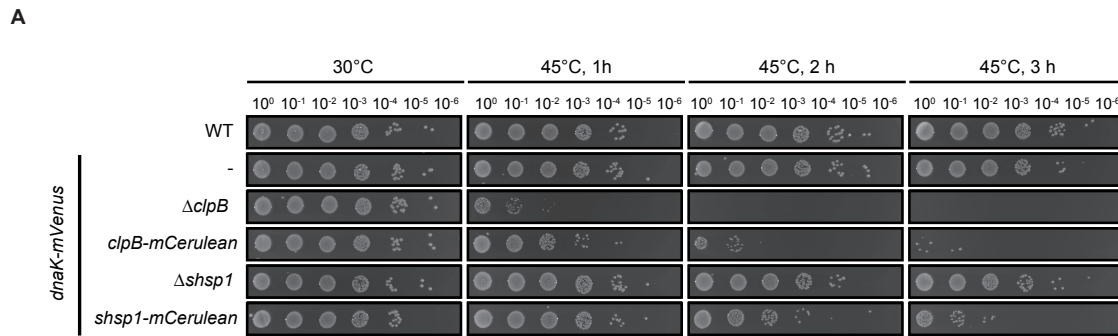
33

**Supporting Information Figure 1. Viability and functionality of the fluorescent reporters used in this study.**

(A) Spot assays showing resistance to exposure of 45°C of the wild type and strains bearing the indicated deletions or fusions in addition to DnaK-mVenus. (B) Microscopy images demonstrating localization of the small heat shock proteins sHSP1 after 1 h at 40°C.
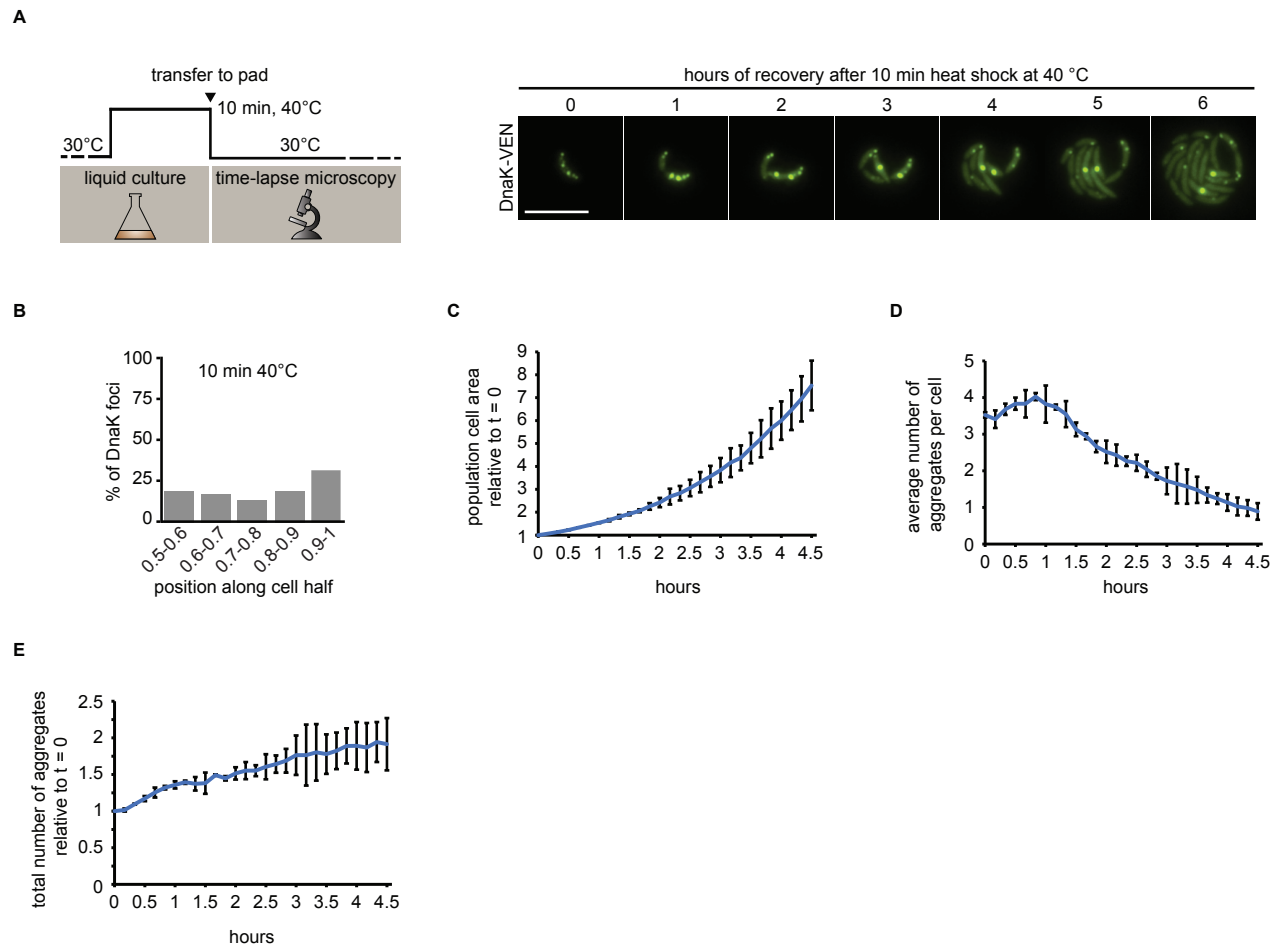
**Supporting Information Figure 2. Δ*clpB* cells recovering from mild heat stress do not dissolve aggregates.**

(A) Schematic of recovery experiment (left) and representative images from Δ*clpB* cell recovery after exposure to 40°C for 10 min. (B) Graph illustrating the position of DnaK-mVenus foci along five bins from midcell (0.5) to the cell pole (1) in Δ*clpB* cells after a 10 min heat shock at 40°C in liquid medium. Quantification based on 313 cells harboring 1056 aggregates. (C) Total population cell area increase relative to the area after stress exposure (t=0). (D) Average number of aggregates per cell over time. (E) Total number of aggregates present in the population over time normalized to time=0. Quantifications in (B-D) show the means of biological duplicates for which 19 microcolonies each were quantified. Error bars represent the standard deviation.

52
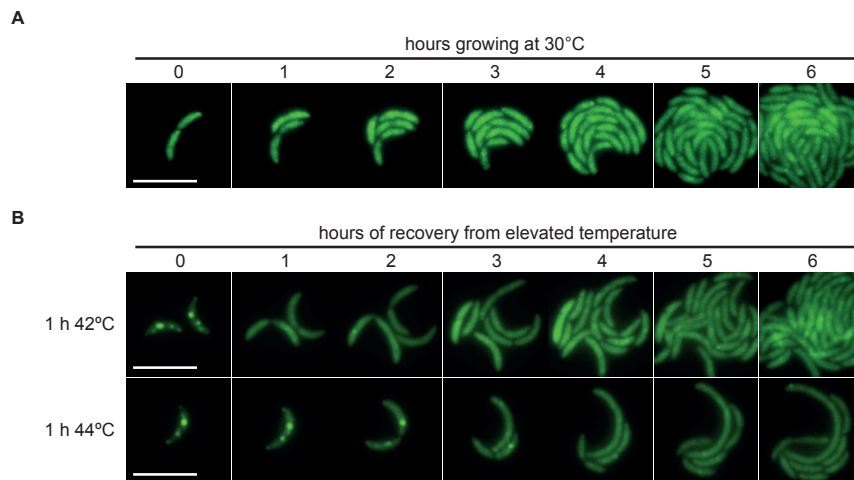
**Supporting Information Figure 3. Representative time courses of cells continuously growing at 30°C or recovering from elevated temperature.**

(A) Representative images of *C. crescentus* grown at 30°C in a heated microscopy chamber over a six hour period. (B) Representative images of *C. crescentus* grown at 30°C in a heated microscopy chamber during recovery from exposure to 42°C or 44°C over a six hour period. Scale bar is 5 μm.

59

**Supporting Information Figure 4. Growth and aggregate clearance in cells recovering from 1 h of exposure to 44°C.**

(A) Scatter plot representing relative area increase, relative aggregate number normalized to the amount present at stress release, and the number of divisions of 22 cells and their progeny after four hours (the time at which the average area of the population has quadrupled) at 30°C after release from one hour of exposure to 44°C. (B) Quantification of aggregate life span in cells recovering from 44°C. Aggregates present or emerging in the first 400 min of a fluorescence time-lapse movie were tracked until 500 min. Images were acquired every 10 min. Quantifications show the means of biological duplicates for which at least ten microcolonies and 94 aggregates each were analyzed. Error bars represent standard deviations.

| original relative position in the mother cell | relative position in stalked daugther after cell division | | |
| --- | --- | --- | --- |
| | closer to new pole | unchanged | closer to old pole |
| old pole | 10%[1]/6%[2]/8%[3] | 90%[1]/94%[2]/92%[3] | N/A |
| old pole half | 34%[1]/58%[2]/81%[3] | 64%[1]/42%[2]/18%[3] | 2%[1]/0%[2]/1%[3] |
| midcell | 71%[1]/78%[2]/66%[3] | 26%[1]/21%[2]/30%[3] | 3%[1]/1%[2]/4%[3] |
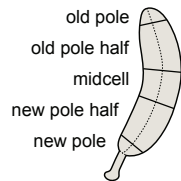
[1]aggregates in Δ*clpB* cells growing at 30°C after exposure to 40°C for 10 min (Fig. 6C)

[2]persistent aggregates in wild type cells (Fig. 4D) continuously exposed to 40°C (Supporting Information Fig. 5)

[3]persistent aggregates in wild type cells (Fig. 4E) recovering at 30°C from 1 h at 44°C (Supporting Information Fig. 6)
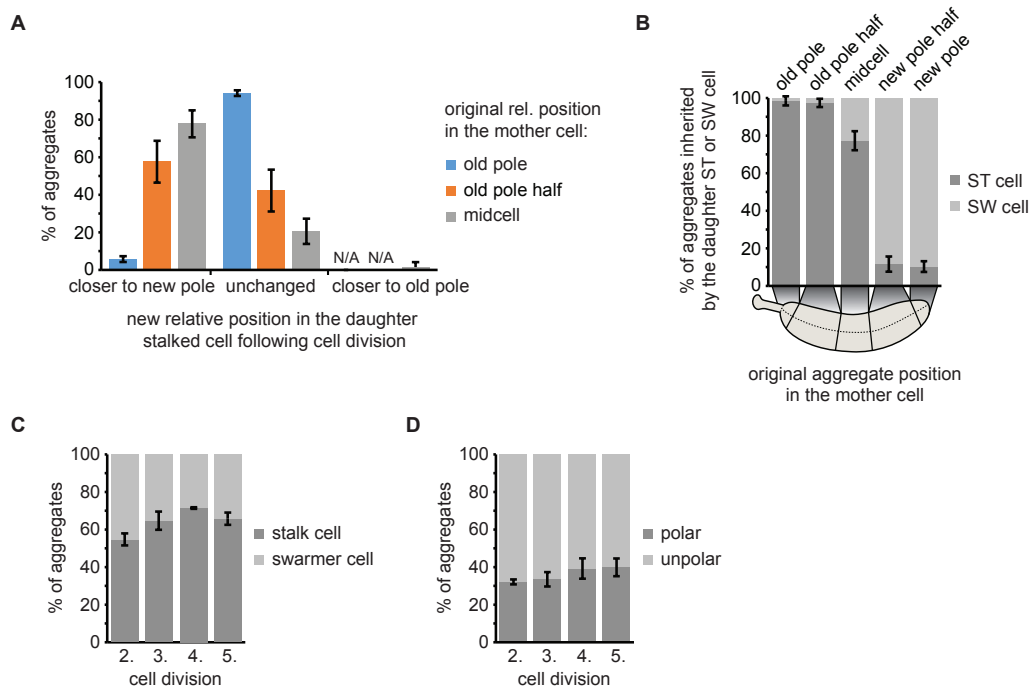
**Supporting Information Figure 5. Schematic table summarizing how positional changes after cell divisions ranked by the position in the mother cell were quantified.**

The table shows how aggregate inheritance was analyzed for generating Figure 6C and Supporting Information Fig. 6A, 7A. Percentage numbers represent the distribution of aggregate positional changes.
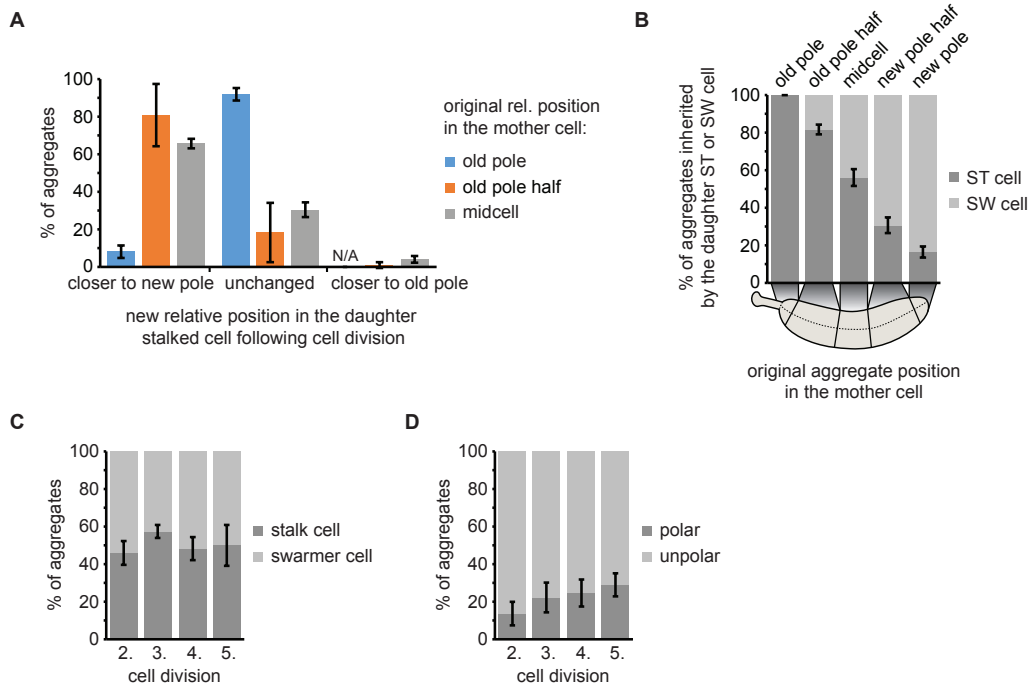
**Supporting Information Figure 6. Inheritance of persistent protein aggregates in DnaK-mVenus cells continuously exposed to 40°C.**

(A) Distribution of aggregates becoming closer to the new pole, remaining stationary or becoming closer to the old pole in the daughter stalked cell, ranked by position in the mother cell. (B) Proportion of aggregates inherited by either a swarmer or a stalked cell as function of their cellular position in the mother cell. (C) Percentage of aggregates inherited by the stalked or the swarmer daughter cell after the second to the fifth division. (D) Localization of aggregates tracked from the second to the fifth division. Aggregate position quantifications resulted from tracking the same population of aggregates from the second to the fifth division. Quantifications are based on biological triplicates for which at least 82 aggregates in at least 21 microcolonies each were tracked. For the quantifications in (A) and (B) the aggregate positional changes after each division were binned leading to at least 246 aggregate positional changes tracked per replicate. Error bars represent standard deviations.

**Supporting Information Figure 7. Inheritance of persistent protein aggregates in DnaK-mVenus cells continuously exposed to 44°C.**

(A) Distribution of aggregates becoming closer to the new pole, remaining stationary or becoming closer to the old pole in the daughter stalked cell, ranked by position in the mother cell. (B) Proportion of aggregates inherited by either a swarmer or a stalked cell as function of their cellular position in the mother cell. (C) Percentage of aggregates inherited by the stalked or the swarmer daughter cell after the second to the fifth division. (D) Localization of aggregates tracked from the second to the fifth division. Aggregate position quantifications resulted from tracking the same population of aggregates from the second to the fifth division. Quantifications are based on biological triplicates for which at least 96 aggregates in at least 85 microcolonies each were tracked. For the quantifications in (A) and (B) the aggregate positional changes after each division were binned leading to at least 288 aggregate positional changes tracked per replicate. Error bars represent standard deviations.

**Supporting Information Text 1**

**Extended description of plasmid construction.**

**Construct for fluorescence reporter tagging of *dnaK* at the native locus (pKJ936):** A fragment containing the upstream homology region (UHR) made up of the last 600 bp of *dnaK* before the stop codon and encoding a GSG linker at the 3'-end was amplified using OFS193/318 from chromosomal DNA. The downstream homology region (DHR) encompassing the 665 bp downstream of the gene was amplified with OFS197/198 from chromosomal DNA. The fluorescence reporter encoding gene *mVenus* was amplified with OFS289/307. The fragments were assembled into *Hind*III/*Eco*RI restricted pNPTS138 by Gibson assembly (Gibson et al., 2009).

**Construct for fluorescence reporter tagging of *clpB* at the native locus (pKJ937):** A fragment comprising the UHR encompassing the last 635 bp of *clpB* before the stop codon as well as encoding a GSG linker at the 3'-end was amplified using OFS287/288 from chromosomal DNA. The DHR containing the 601 bp downstream of *clpB* was amplified with OFS290/291. The fluorescence reporter encoding gene *mCerulean* was amplified with OFS289/307. The fragments were assembled into OFS285/286 amplified pNPTS138 by Gibson assembly.

**Construct for fluorescence reporter tagging of *shsp1* (*CCNA_02341*) at the native locus (pKJ938):** A fragment comprising the UHR encompassing 223 bp upstream of *shsp1* (CCNA_02341), the entire gene except for the stop codon and encoding a GSG linker at the 3'-end was amplified using OFS292/293 from chromosomal DNA. The DHR containing the 594 bp downstream of *shsp1* was amplified with OFS294/295. The fluorescence reporter encoding gene *mCerulean* was amplified with OFS289/307. The fragments were assembled into OFS285/286 amplified pNPTS138 by Gibson assembly.

10

**Constructs for vanillate-dependent expression of mCherry-ELK16 from the chromosomal *vanA* locus (pKJ939):** For the construction of pKJ939 the TP-linker-ELK16 encoding sequence was added to the 3'-end of *mCherry* by sequential PCRs in two steps. First *mCherry* was amplified using OFS308/309 and the resulting fragment was used as a template for an amplification with OFS308/310. The resulting fragment was restriction cloned into *Nde*I/*Xba*I cut pBVMCS-2 resulting in pKJ949. This construct was used as a template to amplify *mCherry-ELK16* which was then restriction cloned into *Nde*I/*Sac*I cut pVCHYN-4 resulting in pKJ939.

**Constructs for xylose-dependent expression of mCerulean-tagged endogenous aggregating proteins from the chromosomal *xylX* locus (pKJ941-943):** For the construction of pKJ941, pKJ942 and pKJ943, the endogenous genes were amplified from chromosomal DNA using OFS865/866, OFS869/870 or OFS880/881, respectively, and assembled with either OFS867/868, OFS871/868 or OFS875/879 amplified *mCerulean* into *Nde*I/*Sac*I cut pXCHYN-1 by Gibson assembly.

**Constructs for deleting chaperone and protease encoding genes (pKJ944-946):** For making pKJ944 the UHR containing the 608 bp upstream and the first 15 bp of *ibpA* was amplified from genomic DNA using OFS795/796. The DHR containing the last 27 bp and the 586 bp downstream of *ibpA* was amplified with OFS797/798. The fragments were assembled with an OFS801/802 amplified *rif^R*-cassette into *Eco*RI/*Hind*III cut pNPTS138 by Gibson assembly. In order to construct pKJ945 the UHR encompassing the 646 bp upstream and the first 15 bp of *ibpB* was amplified from genomic DNA using OFS809/817. The DHR containing the last 27 bp and the 612 bp downstream of *ibpB* was amplified using OFS811/818. The homology region were assembled with an OFS25/26 *tet^R*-cassette (pNPTS-*lon::tet^R*) (Leslie et al., 2015) into *Eco*RI/*Hind*III cut pNPTS138 by Gibson assembly. For the generation of pKJ946 the UHR comprising the 606 bp upstream and the first 15 bp of *clpB* was amplified from genomic DNA

11

156     using OFS803/807. The DHR encompassing the last 27 bp and the 537 bp downstream of *clpB*

157     was amplified with OFS805/808. The homology region were assembled with an OFS25/26

158     amplified *tet^R*-cassette (pNPTS-*lon::tet^R*) (Leslie et al., 2015) into *Eco*RI/*Hind*III cut

159     pNPTS138 by Gibson assembly.

160     **Constructs for ectopic overexpression of *dnaK*- and *dnaK(K70A)-GSG-mVenus* (pKJ950-**

161     **951):** For constructing pKJ950 *dnaK* was amplified from chromosomal DNA with OFS302/303

162     and assembled with OFS289/307 amplified *mVenus* into the OFS300/320 amplified vector

163     pBVMCS-2 by Gibson assembly. In case of pKJ951 the mutation in *dnaK* was introduced by

164     assembling two fragments by Gibson assembly which harbor the desired sequence alteration in

165     the overlapping region. The fragments were amplified using OFS306/320 and OFS305/307,

166     respectively, using pKJ951as template.

167

168     **Extended description of strain construction.**

169     **Fluorescence reporter tagging of DnaK, ClpB and sHSP1 (CCNA_02341) at the native**

170     **locus (KJ952, KJ953, KJ969):** C-terminally tagging chromosomal chaperone genes with

171     fluorescent reporter encoding sequences was achieved by a two-step recombination procedure

172     (Skerker et al., 2005). *C. crescentus* NA1000 was transformed with pKJ936 to generate KJ952

173     or with pKJ948 to generate KJ969. KJ952 was transformed with pKJ937 to generate KJ953.

174     First integrants were selected for by plating on kanamycin-containing plates. Selected

175     integrants were grown over night in PYE medium lacking kanamycin and plated on 3 % sucrose

176     containing plates. Clones being both sucrose-resistant and kanamycin sensitive were verified

177     for plasmid excision and fluorescent reporter gene insertion at the correct locus by colony PCR

178     and fluorescence microscopy.

179

180

181

182    **Vanillate- and xylose-dependent expression of fluorescently tagged artificial and**

183    **endogenous aggregating proteins as well as DnaK-GSG-mVenus from the chromosome**

184    **(KJ955, KJ959-961):** Plasmids encoding for fluorescently tagged artificial, endogenous

185    aggregating and untagged fluorescent proteins under the control of $P_{vanA}$ or $P_{xylX}$ were integrated

186    through homologous recombination at the chromosomal *vanA* or *xylX* site, respectively.

187    Integrants were selected by the plasmid encoded antibiotic resistance and verified by colony

188    PCR. KJ953 was transformed with pKJ939 to generate KJ955. For the generation of KJ959,

189    KJ960 and KJ961, KJ952 cells were transformed with pKJ941, pKJ942 and pKJ943,

190    respectively.

191    **Wt DnaK- and DnaK(K70A)-GSG-mVenus overexpressing strains (KJ956, KJ957):** *C.*

192    *crescentus* NA1000 was transformed with the replicating plasmids pKJ950 and pKJ951 to

193    obtain KJ956 and KJ957, respectively.

194    **Chaperone and protease knockout strains (KJ962-966):** Antibiotic-resistance marked

195    knockouts of chaperone and protease encoding genes were obtained by two step recombination

196    under constant exposure to the antibiotic against which the resistance cassette replacing the

197    deleted gene sequence provides protection. KJ952 was transformed with either pKJ944,

198    pKJ945, pKJ946 or pNPTS-*lon::tet*$^R$ for the generation of KJ962, KJ963, KJ964 and KJ966,

199    respectively. For constructing KJ965, KJ962 was transformed with pKJ945. Clones were

200    verified by colony PCR.

## Supporting Information References

201

202   Gibson DG, Young L, Chuang R-Y, Venter JC, Hutchison CA, Smith HO. 2009. Enzymatic

203       assembly of DNA molecules up to several hundred kilobases. *Nat Methods* **6**:343–345.

204       doi:10.1038/nmeth.1318

205   Leslie DJ, Heinen C, Schramm FD, Thüring M, Aakre CD, Murray SM, Laub MT, Jonas K.

206       2015. Nutritional Control of DNA Replication Initiation through the Proteolysis and

207       Regulated Translation of DnaA. *PLOS Genet* **11**:e1005342.

208       doi:10.1371/journal.pgen.1005342

209   Skerker JM, Prasol MS, Perchuk BS, Biondi EG, Laub MT. 2005. Two-component signal

210       transduction pathways regulating growth and cell cycle progression in a bacterium: a

211       system-level analysis. *PLoS Biol* **3**:e334. doi:10.1371/journal.pbio.0030334

212